# DEGRADATION OF PHENOL BY DYE SENSITIZED NANOPARTICLES

By

**Warda Jabeen**

(Reg#00000277576)

**A thesis submitted in partial fulfillment of requirements for the degree of**

**Master of Science**

**In**

**Environmental Science**

**Institute of Environmental Sciences and Engineering (IESE)**

**School of Civil and Environmental Engineering (SCEE)**

**National University of Sciences and Technology (NUST)**

**Islamabad, Pakistan**

**(2021)**

# DEGRADATION OF PHENOL BY DYE SENSITIZED NANOPARTICLES

By

**Warda Jabeen**

(Reg#00000277576)

A thesis submitted in partial fulfillment of requirements for the degree of

Master of Science

In

Environmental Science

**Institute of Environmental Sciences and Engineering (IESE)**

**School of Civil and Environmental Engineering (SCEE)**

**National University of Sciences and Technology (NUST)**

**Islamabad, Pakistan**

**(2021)**

**Annex A** To. NUST Letter

No 0972/102/Exams/Thesis

Cert Dated_____ August,2021

## THESIS ACCEPTANCE CERTIFICATE

Certified that final copy of MS thesis submitted by **Ms. Warda Jabeen** (Registration No. 00000277576) of **IESE (SCEE)** has been evaluated by the undersigned, found complete in all aspects as per NUST Statutes/Regulations, is free of plagiarism, errors and mistakes and is accepted as partial fulfilment for award of MS Degree. It is further certified that necessary revisions as pointed out by GEC members of the scholar have been also incorporated in the said thesis.

Signature: _____

Name of Supervisor: **Dr. Muhammad Arshad**

Date: _____

Signature (HoD): _____

Date: _____

Signature (Dean/ Principal): _____

Date: _____

It is certified that the contents and form of the thesis entitled

"**DEGRADATION OF PHENOL BY DYE SENSITIZED NANOPARTICLES"**

submitted by

**Warda Jabeen** (Reg#00000277576)

Has been found satisfactory for the fulfillment of partial requirements of the degree of Master of Science in Environmental Science.

Supervisor: _____

Dr. Muhammad Arshad

Professor

IESE, SCEE, NUST

Member: _____

Dr. Zeshan

Associate Professor

IESE, SCEE, NUST

Member: _____

Dr. Khurram Yaqoob

Associate Professor

SCME, NUST

*This thesis is dedicated to my parents*

*for their love and dedicated partnership for success in my*

*life and my friends for their affection and*

*moral support throughout my academic career*

# ACKNOWLEDGEMENTS

*Foremost, I would like to express my earnest gratitude to my advisor* ***Dr. Muhammad Arshad*** *(Associate Professor IESE, SCEE, NUST) for the constant support of my MS study and research, for his tolerance, inspiration, eagerness, and vast understanding. He assisted me throughout the time of research and writing of this thesis. I could not have imagined having a better supervisor and advisor for my MS study.*

*In addition to my supervisor, I would like to thank my Guidance and Examination committee (GEC) members of my thesis:* ***Dr. Zeshan*** *(Assistant Professor IESE, SCEE NUST),* ***Dr. Khurram Yaqoob*** *(Associate Professor SCME, NUST) for their encouragement and insightful comments.*

*I am also grateful to the lab staff of IESE as well as SCME for being accommodative to all my queries and providing support and help through my research work. I am also grateful to my fellow classmates and lab mates in IESE, for the stimulating discussions, moral and practical support especially to my friend Nabia Farrukh Sohail.*

*I would also like to pay my appreciation to my parents and family members for their affection and support, last, but by no means least, I thank my friends at NUST for their support and encouragement thorough out my course work and research.*

**Warda Jabeen**

## Table of contents

## List of Figures

**CHAPTER 2**



**CHAPTER 3**



**CHAPTER 4**

## List of Tables

**CHAPTER 2**



**CHAPTER 4**

## List of Abbreviations

| | |
|---|---|
| XRD | X-ray Diffraction |
| SEM | Scanning Electron Microscope |
| FTIR | Fourier Transform Infrared Spectroscopy |
| $TiO_2$ | Titanium dioxide |
| TNPs | Titania Nanoparticles |
| UV | Ultravoilet |
| BOD | Biological Oxygen Demand |
| COD | Chemical Oxygen Demand |

## Abstract

Compounds well known for their recalcitrant nature are the phenolic ones which produce toxic byproducts in water. They enter the environment from various anthropogenic activities, and they have the ability of undergoing various transformations converting them into even more toxic pollutants. The present study was designed to consider the degradation of phenol by dye sensitized nanoparticles. Dye sensitization of $TiO_2$ nanoparticles was done to increase the photocatalytic activity of $TiO_2$ nanoparticles. $TiO_2$ nanoparticles were synthesized by the liquid impregnation method. Sensitization of $TiO_2$ nanoparticles was done by preparing various concentrations of safranin solutions ranging from $1x10^{-2}$ mM to $5x10^{-2}$ mM and adsorbing the dye by heating at 80°C for 2 h followed by centrifugation and filtration, safranin sensitized nanoparticles were obtained. Characterization of both pure $TiO_2$ nanoparticles and safranin sensitized nanoparticles were done by XRD, SEM and FTIR. Photocatalytic degradation of phenol was done under both ultraviolet (8W & 16W) and visible (18W & 36W) lights at various time periods starting from 0 min to 6 h. Photocatalytic degradation of phenol was also carried out at pH 3 up to 6 h. The results showed that the optimum dosage of 500 mg/ 500 mL safranin sensitized $TiO_2$ nanoparticles degraded the phenol concentration of 50 mg/L up to 60% under 36W of visible light and at pH 3. It was concluded that the efficiency of safranin sensitized $TiO_2$ nanoparticle was enhanced under visible light irradiation due to narrowing of band gap energy.

*Chapter- 1*

# 1 INTRODUCTION

## 1.1 Background

Water is a reusable as well as a renewable resource (Brandao *et al*., 2017) but with the development and establishment of worldwide industries, the threatened resources of water are becoming a serious issue (Chen *et al.*, 2017; Chen *et al*., 2018; Liu *et al*., 2019). Due to heavy industrialization, not only the water resources are drastically declining, but it is becoming responsible for the severe climatic changes (Chopra, 2016). Various industries including textile, paper, and petrochemical industries produce different toxic wastes causing a hazardous impact on environment and also causing life threatening risks to humans, animals and aquatic organisms (Geissen *et al*., 2015).

Petrochemical industries consume a huge amount of water and in result, generate significant volume of wastewater containing oil and grease which is continuously released into the water bodies (Abd El-Gawad, 2014). Out of these discharged pollutants, phenols are one of the most recalcitrant pollutants even after being treated by different methods, which upon digestion by living beings, cause serious health related issues.

According to the present circumstances of water pollution, no promising solution or treatment methods except physical, chemical and biological methods are recognized and accepted, that are not well efficient. So in this regard, serious steps and concerns are required.

## 1.2 Phenol

The effluents released from the industries contain various organic pollutants. Out of these pollutants, compounds well known for their recalcitrant nature are the phenols and they produce toxic byproducts in water (Murcia *et al*., 2020).

Some of the phenolic compounds enter into the environment especially water bodies from many activities such as domestic, industrial, and other agricultural activities resulting in the production of various pollutants. These pollutants have the ability to undergo various transformations which can be due to different reactions with chemical, physical or microbial factors converting them into even more toxic pollutants than their original compounds (Anku *et al*., 2017).

The entrance of phenolic compounds into the soil can be due to the deposition of atmospheric precipitation (in the form of snow and rain), by the application of various herbicides. The solubilized phenols in soil can have the following possible fates (Adeola, 2018).

- Might undergo mineralization and degradation by the heterotrophic microorganism
- Transformation into recalcitrant substances by condensation reactions
- Might remain in forms that are easy to dissolve
- Able to leave the ecosystem as leachate coming from percolating water

Upon exposure to phenolic compounds, human body becomes more susceptible to other toxic pollutants, contact with the body may cause necrosis and skin irritation, and ingestion through drinking polluted water may lead to liver and kidney damage. In animals, inhalation may cause pulmonary, liver, myocardial and renal damage, and also causes dermal effects. While in an aquatic environment, exposure to even little concentration can be toxic and may lead to disruption in the food chain of the aquatic species (Gami *et al*., 2014).

### 1.3 Methods for wastewater treatment

Conventional methods used for the processing of phenolic compounds are:

- Ozonation
- Extraction method
- Biological method
- Ion exchange and adsorption
- Membrane separation based method and
- Photocatalytic degradation

Out of these above-mentioned methods, photocatalytic degradation proves to be the most effective and efficient way of treating phenolic compounds. Although these treatment methods are highly cost effective, but they result in the production of toxic intermediate products (Anku *et al*., 2017).

### 1.4 Proposed solution

To overcome all the limitations of other treatment methods and minimizing environmental contamination, an effective and efficient approach is required. Therefore, many efforts have been made all over the world for the development of an efficient method.

$TiO_2$ is the promising heterocatalyst for the photocatalysis based degradation of phenol. Band gap energy of $TiO_2$ is 3.2eV making it a perfect candidate for photocatalysis (Kanan *et al*., 2020). Under ambient conditions, if the molecules of the safranin dye get adsorbed on the surface of TiO2, then induced by visible portion of light, safranin dye induced $TiO_2$ photocatalyst are attained. As mentioned in various studies, to make the effective use of $TiO_2$ nanoparticles under visible light, dye sensitization is required (Safaralizadeh *et al*., 2017).

Dye sensitization is a simple and new technique that extends the activation of $TiO_2$ to wavelengths that are longer than its band gap energy. This innovative technology has been reported in various studies which plays a crucial role in the efficient and effective degradation of phenols and other organic based pollutants. This technique mainly involves the electron excitation from the excited state of the dye molecule to the $TiO_2$ conduction band followed by formation of electrons ($e^-$) and holes ($h^+$) in the respective bands, leading ultimately to the production of hydroxyl radicals ($OH^-$) responsible in degradation of the phenolic compounds (Chowdhury *et al*., 2012).

Based on a recent study, Ali et al. (2016) used dye sensitized titania nanotubes for the light induced degradation of low-density based polyethylene (LDPE) films, and they were able to achieve degradation of LDPE films using dye induced titania nanotubes through visible light. This study involves the assessment of effectiveness of safranin dye sensitized $TiO_2$ nanoparticles in the phenol degradation.

## 1.5 Objectives

The main objectives of this study were:

- Synthesis of safranin sensitized $TiO_2$ nanoparticles
- To evaluate the effectiveness of dye sensitization on phenol degradation

*Chapter- 2*

# 2 LITERATURE REVIEW

## 2.1 Background

Environmental contamination seems a serious threat for humans and it is increasing day by day. Aquatic pollution is one of the main issues most prominently in the third world countries such as, Pakistan. The enormous spillage and leakage of contaminants from oil and petroleum industries entering into the environment can cause serious negative impacts to the underground water and soil. These impacts may include the contamination of the drinking water along with disturbing the microbial communities in it (Leven *et al*., 2010).

## 2.2 Types of pollutants

The hazardous chemicals which are being released from the effluents coming from petrochemical and chemical industries are mainly responsible for having serious environmental impacts (Al-Khalid *et al*., 2017). Diverse compounds and substances left untreated in the wastewater are dangerous to living beings including humans, animals, and plants. The pollutants released in the wastewater majorly consist of heavy metals, nutrients, organic matter, endocrine disrupters, and microbes are responsible for having serious environmental issues especially causing various diseases in humans (Akpor *et al*., 2014).

The presence of contaminants and organic matter are responsible for providing a media for some of the pathogenic organisms including fungi, viruses, bacteria, and protozoa. These pathogenic organisms are responsible for the arrival of diseases from the contaminated water being released (Akpor *et al*., 2014). These pollutants and contaminants have carcinogenic and mutagenic properties and are considered as primary pollutants by the US Environmental Protection Agency (EPA). The hardly degrading contaminants mostly the phenolic compounds and aromatic organic compounds that are released from the effluents, tend to remain in the environment due to their persistent nature (Al-Khalid *et al*., 2017).

## 2.3 Phenols

The commercial substance known as phenol is involved in the manufacturing industries of pharmaceutical, antiseptic, oil refining, dye reagents, explosives and in the preservatives used in wood. The phenolic compounds act as a colorless substance with crystal structure at room

temperature and absorb moisture in water leading to the hygroscopic property which makes it easy to get leaked or dispersed into the drinking water sources (Gami *et al*., 2014). The main sources of phenol include the oil and petrochemical industries.

The consumption of clean water in oil producing industries and refineries is around 75.7 liters to 227.1 liters, respectively which is used in the processing of almost 1 container of unpolished oil. Out of total water qunatity used, the amount of polluted water produced is 41%. Through various investigations, it was found that the wastewater had Biological Oxygen Demand (BOD) which is about 300 ppm, concentration of mud and oil about 500-3000 ppm, Chemical Oxygen Demand (COD) about 750-1600 ppm, phenol about 80-185 ppm (Al Hashemi *et al*., 2014), concentration of various nutrients including sulphide about 13-17 ppm, ammonia level about 14 ppm and temperature and pH above 30°C and 7, respectively (Azizah *et al*., 2018).

It has been stated that, the extent of phenolic substances varies from 80 to 185 ppm for outer outlet, for the waste stream varies in the range 40-80 ppm and for the common wastewater, it varies in the range of 100 ppm (Al Hashemi *et al.*, 2014). These levels are very high and a continuous threat for environmental health.

The different varieties of pollutants coming out of the industries such as industries of petrochemicals include sulfides, hydrocarbons, phenols, grease and oil and, many other organic and dissolved contaminants which are easily measured by the COD and BOD. The released aromatic hydrocarbons persist in the environment even after going through natural mechanisms and manifest mutagenic and carcinogenic properties. The phenolic compounds are easily soluble in water and can easily enter and contaminate the aquatic environment due to high mobility. Due to the toxic impacts of phenolic compounds, the World Health Organization (WHO) issued guidelines that the phenol concentration in the drinking water should be limited to 1.0 µg/L (Singh *et al*., 2020).

## 2.4 Environmental impacts of phenol

The aromatic chlorinated compounds are known as chlorinated phenols and are frequently present in industrial wastes that are persistent to degradation. The compounds of phenol entering into the soil come from the precipitation of atmospheric deposition in the form of rain and snow causing hazardous impacts on the microbial biota and plants (Adeola, 2018).

By-products of phenolic compounds, such as cresols, exist in water, soil and atmosphere and go through different biological and chemical transformations. They cause serious impacts on the surrounding ecosystem by depleting the dissolved oxygen and, in addition, the by-product cresols limit the oxygen exchange in the aquatic environment thus causing hazardous and toxic impacts on living species such as birds and fishes (Singh *et al*., 2020).

These compounds are known to have deleterious effects on the ecosystem posing toxic impacts on the microorganisms residing in the aquatic environment such as algae, protozoa and it has been reported that higher concentrations of phenol inhibit photosynthetic properties of *Chlorella* sp. While in animals, these compounds are known to cause unfavorable impacts on the nervous and respiratory system, giving rise to numbness and seizures, followed by suffocation (Babich *et al*., 1981).

## 2.5 Health impacts of phenol

In humans, long term exposure and inhalation of phenol is affiliated with cardiovascular, and respiratory diseases such as failure of lungs, kidney and heart. However, contact with the skin may cause skin irritation and damage. Ingestion of phenol causes diseases such as gastrointestinal diseases and ingestion of high concentrations of phenol can even cause death (Public Health Statement, 2008).

Derivatives of phenol including aminophenols, methylphenols, nitrophenols, and chlorophenols, all are known to have toxic impacts on humans. Some alkylphenols are recognized for changing the mammary gland development in mammals and causing endocrine disrupting impacts in humans. In girls, Bisphenol A has the aptness to detain puberty. Exposure and application to higher levels of phenol may cause skin irritation followed by skin burns and may eventually lead to vital organs' disorders. Their capacity to oxidize to by-products which are even more reactive can damage human DNA and proteins present in the body (Anku *et al*., 2017).

Contact with derivative of phenol, pentachlorophenol (PCP), is affiliated with renal and nervous system disorders. Degradation and transformation of PCP can lead to even more toxic compounds that can cause the destruction of DNA. Long term exposure can lead to renal, cardiac and respiratory disorders. Major organs affected by long term exposure to phenol include kidneys, spleen, and pancreas (Adeola, 2018).

Poisoning by cresol leads to severe mouth burning, migraine, low temperature of body, pain in the abdomen, seizures of the nervous system and may even cause the death of human (Singh *et al*., 2020).

## 2.6 Treatment technologies for phenol removal

Numerous technologies that are extensively being used for treatment of pollutants are.

- Physical methods (Adsorption, coagulation, and membrane technologies)
- Chemical methods (Chemical oxidation, ozone treatment, and wet oxidation process)
- Biological methods (Microbial degradation by bacteria and fungi)

Above mentioned methods do not degrade the organic pollutants completely, although these methods transform them into even more recalcitrant pollutants that are difficult to remove. These methods are cost-effective and result in the formation of pollutants at secondary level having cancer-causing or mutagenic properties (Dang *et al*., 2016; Singh *et al*., 2020).

Out of these methods, photocatalysis also known as Advanced Oxidation Processes (AOPs) is the most advanced technique. This technique entirely degrades the organic pollutants into by-products, which are nontoxic like $CO_2$ and $H_2O$ (Shahrezaei *et al*., 2012). Heterogeneous photocatalytic oxidation (HPO) is a new technique employed for the treatment of recalcitrant organic pollutants and produces even less nontoxic substances (Pirbazari *et al.,* 2017). In AOPs, hydroxyl radicals ($OH^{\cdot}$**)** are produced and these radicals take part in the mineralization of different organic pollutants (Singh *et al*., 2020).

## 2.7 Photocatalytic degradation mechanism

Photocatalysis which is also known as AOPs makes use of the semiconductor and UV or Visible light to degrade the organic based pollutants such as phenolic compounds from the wastewater resulting in the production of $CO_2$ and $H_2O$ considered as end products (Singh *et al.,* 2020). The photocatalyic process can be defined as: "A change in the rate of a chemical reaction or its initiation under the action of ultraviolet, visible, or infrared radiation in the presence of the photocatalyst, that absorbs light and is involved in the chemical transformation of the reaction partners" (Braslavsky *et al*., 2007).

A photocatalytic reaction involved in the organic pollutant degradation depends on various factors which are given as follows (Barakat *et al.,* 2014).

- pH

- Concentration and type of organic pollutant
- Type of light (UV or Visible)
- Catalyst loading

In photocatalytic reactions, when a photo catalyst is illuminated with energy that is larger than the photocatalyst band gap, the valence band electrons get excited and jump to the conduction band causing valence band to hold a hole ($h^+$) and causing conduction band to have an electron ($e^-$) (Mahlambi *et al*., 2015). The electrons in excited condition in conduction group will counter with the surrounding oxygen ($O_2$) to generate the superoxide radicals ($O_2^-$), and holes generated in the valence group will interact with water in the surrounding, producing hydroxyl radical ($OH^-$). Both of these produced radicals are responsible for the reaction with the surrounding organic compounds, especially the water-soluble compounds to ultimately degrade the organic compounds into $CO_2$ and $H_2O$ (Diantoro *et al*., 2018).

Photoexcitation

$$TiO_2 + h\upsilon \longrightarrow e^- + h^+$$

Reaction with water

$$h^+ + H_2O \longrightarrow H^+ + HO^-$$

Oxygen isopronation

$$e^- + O_2 \longrightarrow O_2^{-}*$$

Protonation of superoxides

$$O_2^{-}* + H^+ \longrightarrow HOO*$$

The hydroperoxyl radical produced will undergo further reactions, reacting with the electron and hole ultimately producing the hydroxyl radical ($OH^-$), mainly responsible for the organic pollutant degradation (Diantoro *et al*., 2018).

$$R + OH^- \longrightarrow CO_2 + H_2O$$

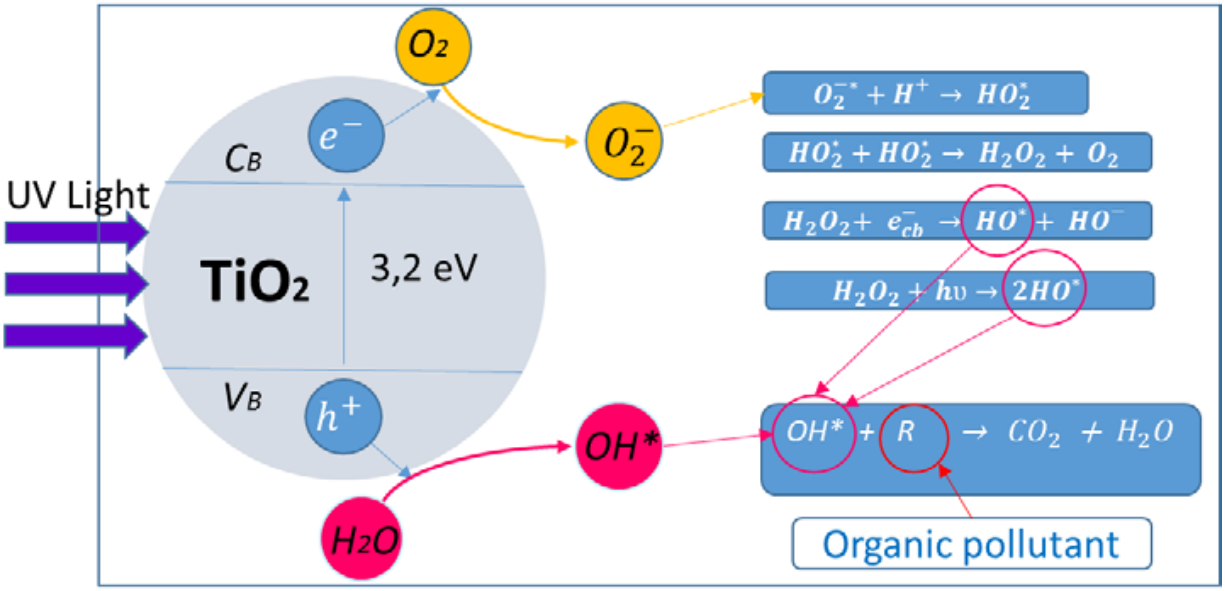


**Figure 2.1 Photocatalytic mechanism of $TiO_2$**

The reactions involving oxidation and reduction both occur at the photocatalyst surface as shown in the Figure 2.1. Diantoro *et al*. (2018) also investigated the photocatalytic processes in various conditions, such as with UV light or visible light and under different pH conditions like in acidic, basic and neutral conditions. Obvious from the results that the photocatalytic based activity of $TiO_2$ nanoparticles will increase under alkaline conditions but the photocatalytic activity will decrease under acidic pH. Results concerning the degradation of phenol by dye sensitized nanoparticles should be high under alkaline conditions as compared to acidic conditions.

## 2.8 Photocatalyst

The most prominent characteristic of a semiconductor photocatalyst is that it is capable of reversing the change being made in the valence band so it can easily accommodate a hole without destroying the semiconductor. In addition, the band gap of the semiconductor photocatalyst must be highly stable, should be nontoxic, should be cost efficient and should have non-corrosive property (Mahlambi *et al*., 2015). Types of semiconductor majorly used in the photocatalytic processes include catalysts such as $TiO_2$, $Fe_2O_3$, GaP, $TiO_2$ and ZnS. Out of these catalysts, $TiO_2$ is the most suitable semiconductor photocatalyst (Dang *et al*., 2016).

### 2.8.1 $TiO_2$ as a photocatalyst

In addition, the property of having an appropriate gap band energy, the polymer should be ideal with the following properties (Gupta *et al*., 2011).

- Easy to produce
- Cost efficient
- Environment friendly
- Stable to light and should get easily excited by light
- Non-toxic to environment and humans

In view of all the above-mentioned properties, $TiO_2$ is a photocatalyst ideally used for the photocatalytic based treatment of contaminants and can be used for many other wide applications. In the family of transition metal oxides, titanium dioxide ($TiO_2$) is a well-known metal oxide.

The photocatalysis by the $TiO_2$ was firstly defined in 1972 by Fujishima and Honda and was stated as "Honda- Fujishima Effect". The well-known process involved the electrolysis of water (Gupta & Tripathi, 2011). $TiO_2$ is known for possessing high optical properties and getting easily activated by UV illumination and making it able to make use of the UV light for the photocatalytic reactions and causing the organic pollutants degradation especially the phenolic compounds (Mangrola *et al*., 2012). As $TiO_2$ has a band gap energy of 3.2ev, its ability to absorb light is limited to the region of UV due to its narrow band gap energy (Safaralizadeh *et al*., 2017).

$TiO_2$ is generally used for the light induced treatment of organic contaminants due to its well-known properties such as (Dang *et al*., 2016):

- Low cost
- Nontoxic and non-corrosive property
- Stable nature
- High chemical and physical stability
- High efficiency
- Extensive availability and
- High photocatalytic activity

Because of all the above-mentioned applications, $TiO_2$ is broadly used for the photocatalytic organic pollutant degradation, especially the phenolic compounds (Barakat *et al*., 2014; Levchuk *et al*., 2020; Singh *et al*., 2020).

### 2.8.2 Polymorphs of $TiO_2$

In the family of transition metal oxides, $TiO_2$ is an important metal oxide. The three commonly identified polymorphs of $TiO_2$ are: anatase (tetragonal), brookite (orthorhombic) and rutile (tetragonal). The anatase phase is usually metastable as compared to other polymorphs and due to higher mobility of electrons, it is used for solar applications (Gupta & Tripathi, 2011). Although, rutile phase is stable phase in comparison to anatase and brookite as both are metastable. Brookite phase synthesis is difficult, so it is the reason that this phase is rarely studied or used in various studies (Hanaor & Sorrell, 2011).

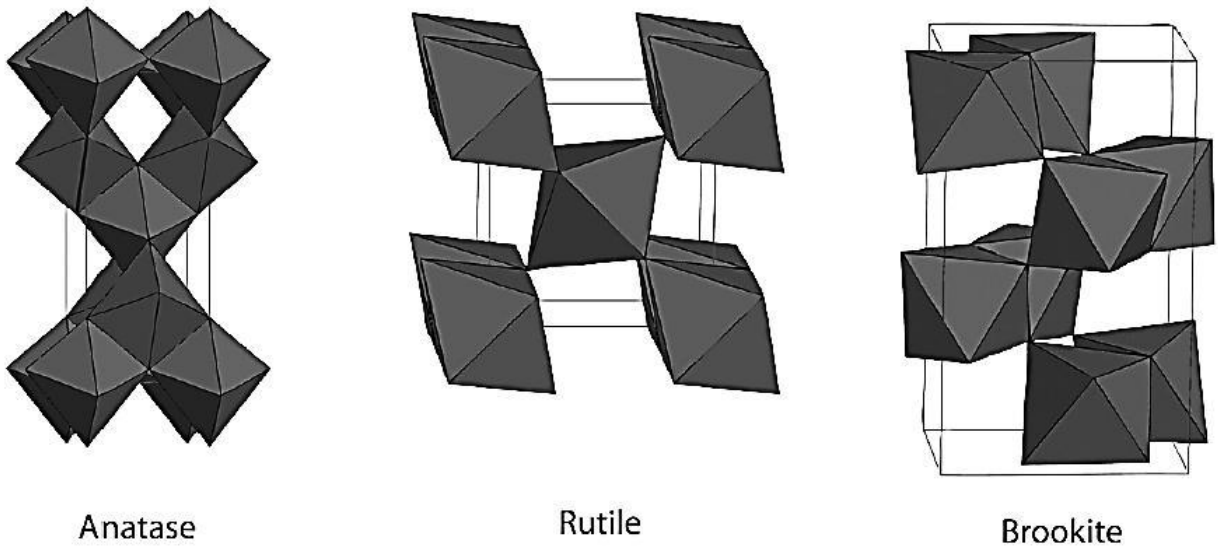


**Figure 2.2: Crystaline arrangement of $TiO_2$ polymorphs (a) Anatase (b) Rutile (c) Brookite (Eskandarloo & Badiei, 2014)**

Instead of various properties and stabilization of anatase phase, it is challenging to retard the change of anatase phase to rutile phase. However, it is reported by Setiawati and his coworkers in 2008, that the addition of $Eu^+$ and $Sm^+$ makes the anatase phase stable (Theivasanthi & Alagar, 2013).

Polymorphic forms of $TiO_2$: Anatase, rutile and brookite phase can be synthesized by following various methods such as (Riaz & Naseem, 2015):

- Sol-gel method
- Sonication method
- Spray pyrolysis method

### 2.8.3 Limitations of $TiO_2$

About only 3.5-8% of solar spectrum consists of UV range and due to larger energy of band gap of $TiO_2$, $TiO_2$ gets only irradiated by the portion of UV, which makes it cost effective and cannot be used for large scale applications. The main drawback of $TiO_2$ as a photocatalyst is that it cannot make use of visible light due to the larger $TiO_2$ band gap. It cannot be irradiated by the visible light and makes it unable for various applications (Chowdhury *et al*., 2012). An urge to establish a modified and an efficient method is required which can cause reduction in the energy of band gap for efficient usage of visible portion light for the light enhanced degradation of organic pollutants.

## 2.9 Titania nanoparticles

Nanoparticles come under the domain of nanotechnology dealing with the science and technology at sizes approximately from 1 nanometer - 1000 nanometers (One meter= billion nanometers), however the suitable dimension for various applications and textile related products is 100 nanometers (Sarathi & Thilagavathi, 2009). Titanium dioxide nanoparticles are known to be highly effective as a photocatalyst due to high stability and efficiency. These particles reveal the distinct properties that when their band gap increases with decrease in particle size, the smaller particles have higher surface area thus increasing the reactivity of particles (Khan *et al*., 2013). $TiO_2$ is known for its various applications such as, sterilization of virus, removal of environmental pollution, making of white toothpaste, as a photocatalyst, development of environmentally friendly products such as self-cleaning fabrics and tiles (Rezaei & Mosaddeghi, 2006). They can be synthesized by various methods.

### 2.9.1 Titania nanoparticles synthesis

Different methods by which $TiO_2$ can be synthesized are as follows (Eskandarloo & Badiei, 2014):

- Sol- gel based process
- Solvo-thermal process
- Liquid impregnation process
- Hydrothermal process
- Wet chemical based process
- Electrochemical process

Liquid impregnation method only involves the addition of one chemical (powder titania) and distilled water. Hence, it is cost efficient, easy method to synthesize $TiO_2$ nanoparticles and easy to handle (Behnajady *et al*., 2009).

### 2.10 Dye sensitization as a modification

The visible light coming from the sun is in the range of 20-30 $Wm^{-2}$ and consists of the major portion of sunlight. The band gap of $TiO_2$ is larger which makes it difficult to get excited by the visible light due to the larger wavelength (400-700nm) but $TiO_2$ becomes active under UV light but the usage of UV light at large scale is very challenging (Ahmed *et al*., 2010). To overcome this problem, several strategies have been developed comprising metal doping, dye sensitization and doping and capping of $TiO_2$ with various metal or nonmetals (Gupta & Tripathi, 2011).

Most of these above-mentioned methods are time consuming and highly expensive. But the modification through dye sensitization, is a simple and new method that can narrow the band gap energy corresponding to the longer wavelength (Chowdhury *et al*., 2012). Modification developed for the effective utilization of the visible light involves dye sensitization of the $TiO_2$ particle which is based on both the chemical or the physical adsorption of the molecules of different dyes on surface of photocatalyst as shown in Figure 2.3 followed by the chemical reaction of the hydroxyl group ($OH^-$) with the organic compound resulting in treatment of the organic based pollutant (Zangeneh *et al*., 2015).

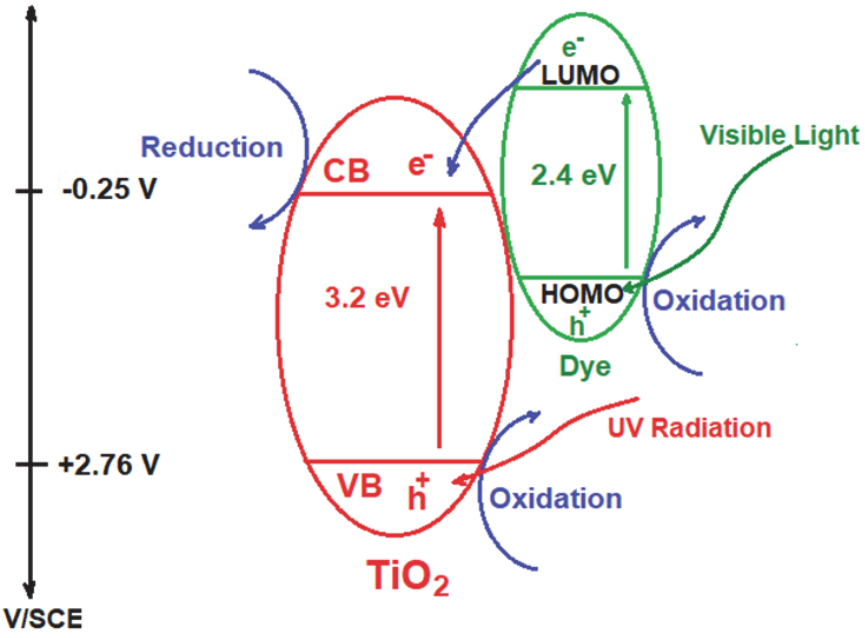


**Figure 2.3 A diagram displaying the sensitization process of $TiO_2$ in photodegradation (Zyoud et al., 2018).**

## 2.11 Previous work on the photodegradation of phenol by dye sensitized nanoparticles

The key advantageous impact of the presence of the bonded or adsorbed dye on the surface of the photocatalyst is because of its ability to absorb or make use of the visible light of solar spectrum for a definite range of wavelength. Mele et al. (2002) reported the difference in the degradation of 4-nitrophenol by $TiO_2$ particles modified by Cu (II)-phthalocyanine and bare $TiO_2$ particles. Results showed the effective 4-nitrophenol degradation by the impregnated $TiO_2$ by Cu (II)-phthalocyanine in comparison to the bare $TiO_2$ samples. Similarly, Granados et al. (2005) stated that sensitized $TiO_2$ with Co (II) and Zn (II) tetracarboxyphtalocyanine (TcPcM) presented the effective light induced degradation of phenol in presence of the region of visible light. Deposition of platinum (Pt) on TcPcM/$TiO_2$ enhanced the light efficiency of the reaction upto $\eta \approx 0.1$.

In another study Chowdhury et al. (2012) used Eosin Y dye sensitized $TiO_2$ with platinum as a co-catalyst in visible region and outcomes exhibited that almost 93% of phenol was degraded by the Eosin Y sensitized $TiO_2$ catalyst. Dai et al. (2014) stated that the use of bacteriorhodopsin sensitized $TiO_2$ nanoparticles for the light induced phenol degradation and percentage of degradation was increased 3.5 times by the sensitized $TiO_2$ nanoparticles as compared to the $TiO_2$ nanoaprticles alone.

Janitabar Darzi & Movahedi (2014) used the modified ZnO and $TiO_2$ nanoparticles with membromin dye for the light induced phenol degradation. After 4 hours, the membromine modified ZnO nanoparticles completely degraded the phenol and on the contrary modified $TiO_2$ nanoparticles only degraded phenol up to 47%. The reason is the less aggregation of the dye molecules on the surface of ZnO nanoparticles caused the excitation of molecules of the dye on ZnO surface for a prolonged lifetime (Janitabar Darzi & Movahedi, 2014).

In another study, sudan black was used as a dye for the sensitization of $TiO_2$ nanoparticles for light induced degradation of phenol using visible region of light and sudan black sensitized $TiO_2$ nanoparticles caused the degradation of phenol upto 96% in 100min period (Safaralizadeh *et al*., 2017). So, safranin dye could help in the excitation of $TiO_2$ and increase the degradation efficiency of organic pollutants like phenol.

### 2.12 Safranin dye

Safranin-O (3,7-diamino-2,8-dimethyl-5 phenylphenazinium chloride) is a phenazine dye which is widely utilized in energy transfer and electron reactions as a photosensitizer and the phenazine dye are widely used in textile industries (El-kemary & El-shamy, 2009). The chemical formula of Safranin O dye is $C_{20}H_{19}N_4Cl$ (Balaji *et al*., 2011).

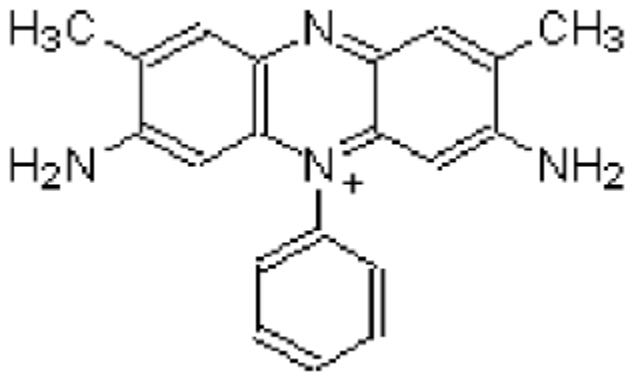


**Figure 2.4 Chemical structure of Safranin O dye (Balaji et al., 2011)**

In the Safranin O dye, $N^+ Cl^-$ group will form a bond with the surface of metal oxide by offering a proton to the lattice of the metal oxide (Kumar *et al*., 2018).

## 2.13 Kinetics of reaction

To quantify the heterogeneous photodegradation activity of the organic compounds, the Langmuir-Hinshelwood is considered:

$$-\frac{dc}{dt} = \frac{kKC}{1+KC}$$

In the above equation, k is constant of photo degradation and K is thermodynamic adsorption rate constant of reaction, t is time and C is the reactant concentration.

The kinetics of the phenol degradation by the $TiO_2$ nanoparticles follows the Langmuir-Hinshelwood equation as follows:

$$-\frac{dC_{Ph}}{dt} = \frac{W}{V} I_{\alpha}^{\beta} \frac{k_r C_{Ph}}{1+K_A C_{Ph}^0} \quad (1)$$

Where $K_A$ is constant of adsorption equilibrium, $k_r$ is constant of kinetic rate, β is constant, V is reaction mixture volume, I is light intensity, W is catalyst mass and $C_{Ph}$ is phenol concentration. Subscript 0 represents initial concentration. Equation 2 represents the apparent kinetic constant as:

$$k_{app} = \frac{W}{V} k_r K_A \quad (2)$$

After combining the equation 1 and 2, we will get:

$$-\frac{dC_{Ph}}{dt} = r_s = I_{\alpha}^{\beta} \frac{K_{app} C_{Ph}}{1+K_A C_{Ph}^0} \quad (3)$$

For the prediction of various kinetic based parameters of photodegradation of phenol at various intensities equation 3 can be used (Chowdhury *et al*., 2012).

## 2.14 Effect of operative parameters on phenol degradation

### 2.14.1 Effect of catalyst loading

The most significant parameters in the phenol degradation is the dosage of the photocatalyst and this parameter has been widely investigated and reported. The concentration of the catalyst not only effects the process efficiency but also the rate of the organic compounds degradation (Bukhari *et al*., 2019).

With increase in catalyst concentration, the total active sites increase, causing increase in hydroxyl ($OH^-$) radicals. The initial reaction rate increases proportionally with increase in the catalyst concentration but after specific point, rate of reaction became constant and independent of concentration of catalyst (Chowdhury *et al*., 2012).

The main reasons for the limiting value of the reaction may be due to: (i) high concentration of the catalyst causes the agglomeration which decreases the active sites (ii) due to higher catalyst concentration, the turbidity of solution increases which reduces transmission of light through the solution, thus, reducing the degradation efficiency of the process (Shahrezaei *et al*., 2012). Previous studies have investigated the degradation of phenol by taking various concentrations of the catalyst which is shown in form of table 2.1

**Table 2.1 Catalyst loading effect on phenol degradation**

| **Pollutants** | **Photocatalyst** | **Verified catalyst loading (g/L)** | **Optimum loading (g/L)** | **References** |
|---|---|---|---|---|
| Phenol | $Pt/TiO_2$ | 0.25- 2.0 | 0.5 | Barakat *et al*., 2014 |
| Phenol | $EY\text{-}TiO_2/Pt$ | 0.1-2.2 | 0.8 | Chowdhury *et al*., 2012 |
| p-cresol | $TiO_2$ | 1.0-3.0 | 1.0 | Singh *et al*., 2020 |

### 2.14.2 Effect of light intensity

Extent of adsorption of light by catalyst of semiconductor determines the light intensity for a given wavelength. Initiation rate for the formation of the electron-hole pair in the photochemical process is highly based on light intensity (Ahmed *et al*., 2010). The intensity of light to be incident is considered to be a rate-controlling parameter (Chowdhury *et al*., 2012). When mass transfer is low with the high intensity of light, the rate of reaction is proportional to the square root of intensity of light. Although, at lower intensity of light, the rate of photodegradation is linearly related to the

light intensity (Chowdhury *et al*., 2017). Various studies have been stated for photo-degradation of organics using either visible light or UV light.

Li Puma et al. (2002) tested impact of light intensity on photodegradation of 2-chlorophenol (2-CP) through concurrent UV-A, along with UV-B and UV-C irradiation. The primary rate of the photodegradation of 2-CP increased 1.8 times with UV-A along with UV-B and UV-C radiation in comparison to alone UV-A radiation. Higher photon flux stood responsible for the improved degradation of 2-CP with UV-A along with UV-B and UV-C in comparison to UV-A radiation (Ahmed *et al*., 2010).

Another study was degradation of 2-Chlorophenol in a photoreactor was evaluated by using different lamps ranging from 20-150 W energy. It was seen that the efficiency of the photodegradation was increased from 3 to 5 folds with 70W and 150W lamps, respectively. 2-CP was completely degraded under 150W lamp within 3h (Rashid *et al*., 2014). Suzuki et al. (2015) stated the combined result of ozone, $TiO_2$ along with UV for phenol photodegradation. It was concluded that almost 100% of the 50 mg/dm$^3$ phenol was degraded within 2h and the removal of COD achieved was 100% within 4h with the combination of ozone, $TiO_2$ and UV process. Chowdhury et al. (2012) studied the dye sensitized $TiO_2$ using visible light and Eosin Y as a dye sensitizer was used. Almost 93% of 40 mg/L phenol degradation was attained in 90 min with visible light having the intensity of 100 mW/cm$^2$. Some studies are reported in table 2.2.

**Table 2.2 Effect of light intensity on phenol degradation**

| Catalyst | Phenolic pollutant | Light source | Degradation Efficiency (%) | References |
|---|---|---|---|---|
| $TiO_2$/Gr/PW | Phenol | UV light | 91% | Rafiee *et al*., 2016 |
| $TiO_2$/Zeolite composite | Phenol | UV light | 100% | Sulaiman *et al*., 2017 |
| N,S codoped $TiO_2$ | Phenol | Visible light | 100% | Yunus *et al*., 2017 |

| | | | | |
|---|---|---|---|---|
| N-$TiO_2$/$SiO_2$/$Fe_3O_4$ | Phenol | Visible light irradiation | 64% | Vaiano *et al*., 2016 |

### 2.14.3 Effect of pH

In the process of photocatalysis, pH parameter shows a significant impact. For $TiO_2$, point of zero charge is around 6.8. Therefore, at basic pH (pH 9.0), the $TiO_2$ surface is charged negatively and at acidic pH (pH 5.0), the $TiO_2$ surface is charged positively. Results showed that the pH had major impact on photodegradation. Under both high and low pH, the rate of photodegradation is relatively less. At pH 5.0, only 28% of phenol degraded that was near to results achieved at pH 9.0 (31% phenol degradation). The optimum pH for the efficient degradation of phenol was 7.0 and almost 100% of the phenol was degraded within 2h (Chowdhury *et al*., 2012).

Rashid et al. (2014) varied the solution pH to study pH impact on the 2-Chlorophenol (2-CP) degradation. It showed that the degradation of 2-Chlorophenol linearly increased with the increased pH upto pH 5.0. And causing further increase in pH upto 7.0, caused a major decreased in the degradation of 2-CP. The electrostatic based binding of 2-Chlorophenol with the positive surface of $TiO_2$ is responsible for the complete degradation of 2-Chlorophenol. Wang et al. (2017) stated the impact of pH on degradation of phenol. At initial stage, highest degradation obtained was at pH 1.0 and then noticeable decrease in phenol degradation was noticed with increasing pH, maximum degradation achieved was 92.4%. The results showed that phenol degradation were favored in the low pH and on other hand, it was repressed in the basic pH in comparison to the neutral pH. It is considered that the phenol is in its nonionic form in the acidic condition leading to high density production of hydroxyl radicals ($OH^-$) near to $TiO_2$ catalyst surface.

This study is based on cited literature and is studied under different operative parameters like effect of dosage of catalyst, light and pH. The selected dye (safranin) could help in increasing the efficiency of $TiO_2$ nanoparticle and make it effective for purpose of degradation of phenol upon dye sensitization.

*Chapter- 3*

# 3 MATERIAL AND METHODS

## 3.1 Materials

Titania general purpose reagent was used for the synthesis of pure $TiO_2$ nanoparticles (TNPs). Chemical $TiO_2$ was purchased from the local market and was used in the preparation of the precursor $TiO_2$ nanoparticles by the liquid impregnation liquid method. Phenol chemical in solid form and safranin dye was also purchased from the local market. For the synthesis of $TiO_2$ nanoparticles analytical grade chemicals and Pyrex glassware was used. De-ionized water was used for all the experiments.

For the light induced degradation of the phenols, 4 visible (ranging from 400-700 nm) and 4 UV lamps (ranging from 280-320 nm) having 18W and 8W energy were used as a light source, respectively. UV-Vis spectrophotometer technique was used for the analysis of the phenol degradation.

## 3.2 Method for the synthesis of TNPs

### 3.2.1 Liquid impregnation method

For the synthesis of TNPs, 20g of the titanium powder was made soluble in 100 mL of deionized water in beaker of glass and stirred magnetically for 24 h on hot magnetic plate. Resulting mixture was allowed to settle for 24 h followed by oven drying at 105° C temperature for time period of 12 h. Dried sample was crushed with pestle mortar followed by placing in muffle furnace at 550° C for 6 h to obtain the titania nanoparticles (Husnain *et al*., 2016). The nanoparticles were cooled at room temperature and the particle size of the nanoparticles were from 20 nm to 60 nm with average size of 36nm. Flow diagram for the preparation of $TiO_2$ nanoparticles is shown in Figure 3.1.

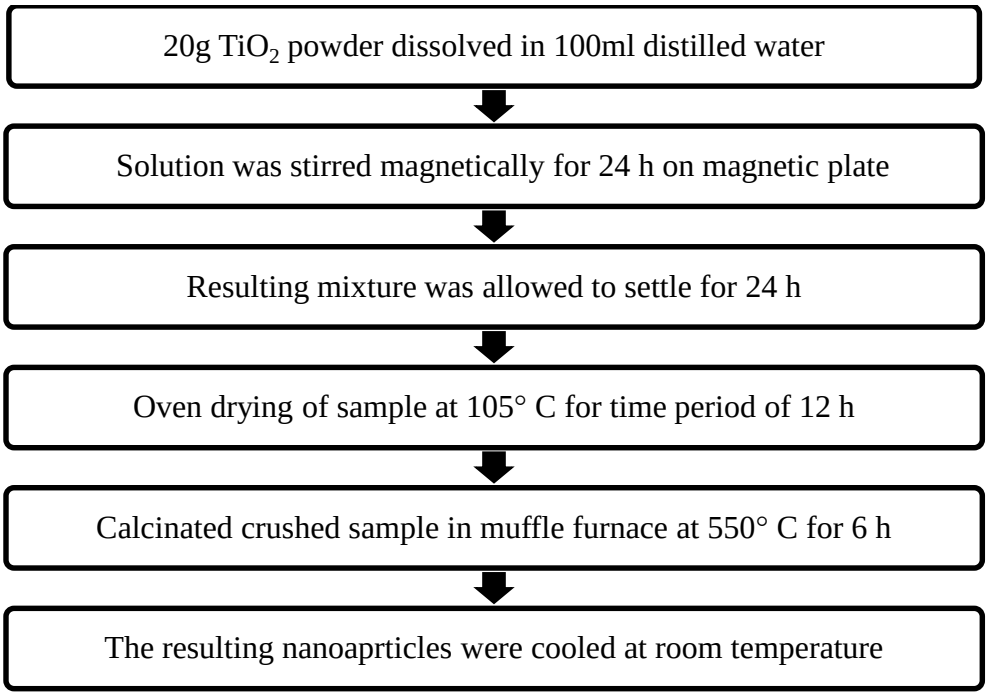


**Figure 3.1 Flow diagram of $TiO_2$ nanoparticles preparation**

### 3.3 Preparation of dye sensitized TNPs

First of all, safranin solutions from $1x10^{-2}$ mM to $5x10^{-2}$ mM were prepared in isopropyl alcohol (Kumar *et al.*, 2018) and the calculated quantity of TNPs were added in prepared solution and pH was adjusted at 3 by adding 0.1 M HCL. The solution was placed for 24 h (Safaralizadeh *et al*., 2017) and the solution was refluxed for 2 h at 80°C so that the dye could fix at the nanoparticles. The dye sensitized nanoparticles were centrifuged and filtered via filter paper (Granados *et al*., 2005). Hence, safranin sensitized nanoparticles were obtained. Flow diagram for the preparation of safranin sensitized nanoparticles is shown in Figure 3.2.

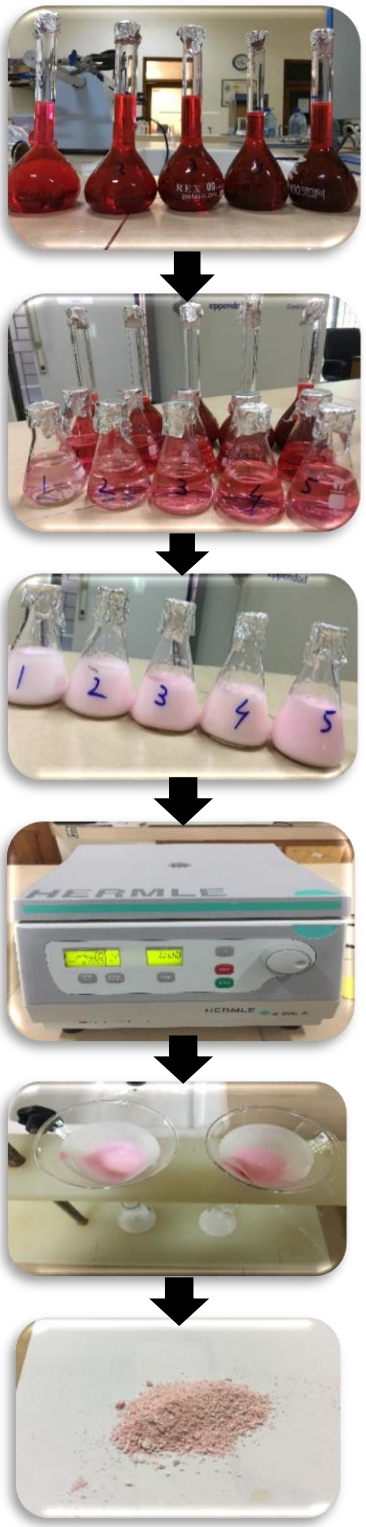

Solutions ranging from 1mM to 5mM was prepared in 100ml volumetric flasks

Dilutions ranging from $1x10^{-2}$mM to $5x10^{-2}$ mM were prepared in 50ml conical flasks

Calculated quantity of $TiO_2$ nanoparticles were added

After heating for 2h at 80°C in oven the particles were centrifuged at 6000rpm for 10min

Particles were separated by the filter paper and oven dried

After oven drying, safranin sensitized nanoparticles were obtained

**Figure 3.2 Flow Diagram of Safranin Sensitized Nanoparticles**

## 3.4 Characterization of $TiO_2$ nanoparticles and dye sensitized nanoparticles

Keeping in view the importance of the crystal size and morphology of nanoparticles in their various applications, characterization of nanoparticles becomes very important for the determination of particle size, texture and shape. Usually, the techniques involved in the characterization of nanoparticles are X-ray Diffraction (XRD), Scanning Electron Microscope (SEM) and Fourier Transform Infrared Spectroscopy (FTIR) tecnhniques (Dil *et al*., 2019; Diantoro *et al*., 2018). By using these characterization techniques, the various properties of nanoparticles such as particle size, particle arrangements, crystallinity of nanoparticles and shape of nanoparticles can be determined. Uniformity, agglomeration and spherical properties of safranin sensitized nanoparticles were determined by SEM (Safaralizadeh *et al*., 2017). XRD is useful for the determination of crystallinity and phase structure of nanoparticles (Dil *et al*., 2019).

### 3.4.1 Scanning Electron Microscope (SEM)

Scanning Electron Microscope tecnhnique or SEM analysis has worldwide known applications in many fields. In the study of inorganic and organic materials, SEM is usually recognized as an operational method with a scale ranging from nanometer to micrometer (μm). SEM can create very accurate images of various materials with a magnification power of 30,000X and as high as 100,000X. This device of SEM also helps in the analysis of samples having diameter up to 200 nm along with a height of 80 mm. Materials having organic and inorganic solids including polymers and metals can be used in SEM for analysis (Mohammed & Abdullah, 2019). The working principle of SEM is shown in Figure 3.3.

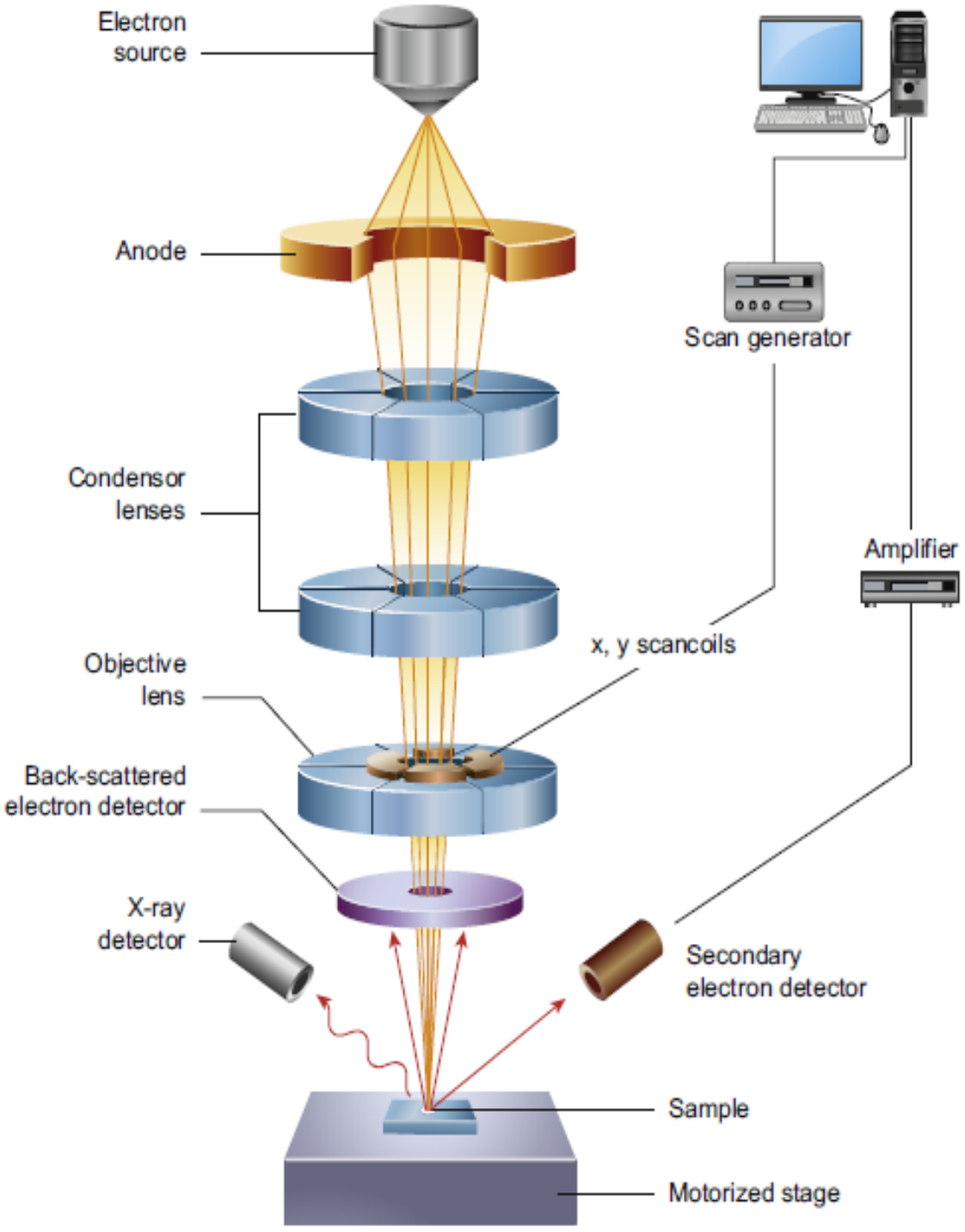


**Figure 3.3 Diagram of the core components of SEM (Inkson, 2016)**

By the application of electron beam, the analysis of sample was done. The range of the electron in the beam lies between 100-30,000 electron volts. The source of electron emission is usually thermal. SEM can compress the spot produced by the electron beam to produce a sharp and accurate image and can also direct the electrons being focused on the sample. The electron detector then detects the emitted electrons from the scanned specimen. The signals are then shown on the screen and the intensity and brightness can be controlled by the operator till a clear and sharp image is achieved. For the analysis of small details, the magnification as high as 100,000X can be applied (Mohammed & Abdullah, 2019).

In this study, size of particle with morphology of titania nanoparticles and the safranin sensitized nanoparticles was done by Sacnning Electron Microscope (JEOL JSM-6490A) at an acceleration voltage of 20kV.

### 3.4.2 X-ray Diffraction (XRD)

In 1912, Max von Laue and Co. found that matters having crystalline nature behave as three-dimensional diffraction gratings for those having plane spacing in crystal lattice equal to the x-ray wavelength. For the study purpose of atomic spacing and crystal structure of various samples, X-ray Diffraction (XRD) technique is a very common method. Working of XRD is based on constructive interference of monochromatic x-rays and that of the crystalline nature based sample. Cathode ray tube is responsible for production of x-rays which are further filtered to generate monochromatic radiation and after being concentrated, it is directed towards the sample. Constructive interferences are produced when the incident radiations counters with the sample which completely meets Bragg's law:

$$n\lambda = 2dsin\theta$$

As $n$ is an integer, $d$ is the interplanar spacing producing the diffraction, θ is angle of diffraction and λ is x-rays wavelength. By scattering the sample thorough 2θ angles, because of random alignment of the powdered crushed sample possible diffraction directions of lattice can be attained. Identification of the sample compound can be carried out by transforming the diffraction peaks into d-spacing as every compound consists of a set of distinctive d-spacing. The x-ray diffractometers consist of (Bunaciu *et al*., 2015):

- Tube of a x-ray

- Holder for sample and
- Detector for x-ray

As shown in Figure 3.4 principle of incident x-rays is displayed. The x-rays interact with the electrons in the sample and are get scattered elastically. Then the scattered waves interfere with each other coming from many atoms and if they are in one plane, then they would interfere constructively. The information in these diffracted x-rays is related to the electron distribution in the materials.

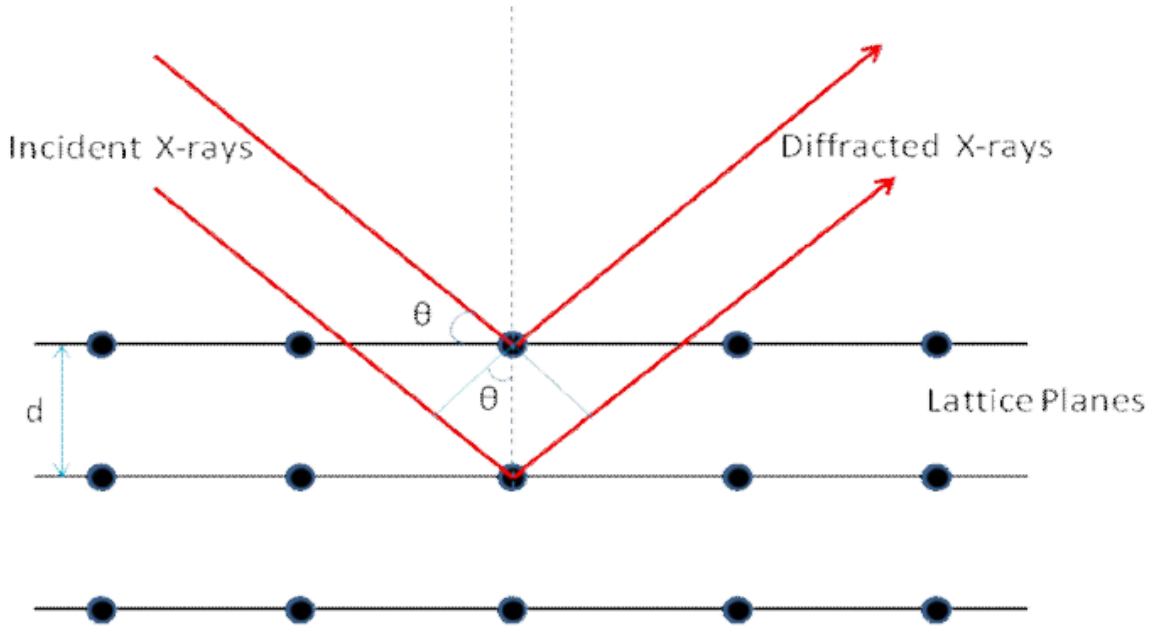


**Figure 3.4 Diffraction of X-rays at Crystal Lattice (Zang &Kumar, 2008)**

The size range of crystals of $TiO_2$ nanoparticles were determined by using the Debye-Scherrer equation:

$$d = \frac{k\lambda}{\beta cos\theta}$$

Where $d$ is the crystalline size of nanoparticle, $k$ is constant for spherical particles (0.9), λ is wavelength of the source the X-ray used (λ=0.154056 nm), $\beta$ is full width half maxima (FWHM)

and θ is angle at the maximum diffraction curve intensity (Safaralizadeh *et al*., 2017). By inserting all the values from the XRD graph, the crystalline size of nanoparticles can be calculated.

### 3.4.3 Fourier Transform Infrared Spectroscopy (FTIR)

To overcome challenges faced with dispersive instruments, Fourier Transform Infrared Spectroscopy (FTIR) technique was developed. Main challenge faced was the slow process of scanning. So, there was a need for the measurement of individual frequency, rather than all the infrared frequencies. Simple optical device was developed as a solution known as interferometer. Unique type of signal consisting of all the infrared frequencies encoded is produced by the interferometer. In a period of almost one second, the signal produced can be measured (Griffiths & De Haseth, 2007).

In the field of organic chemistry, Infrared spectroscopy is a significant technique. By this technique, the identification of certain functional groups in various molecules is done very easily. The study done by the infrared spectroscopy showed the principle that each molecule has specific frequencies of internal vibrations. The range of frequencies occurring in the infrared region varies from ~4000cm$^{-1}$ to ~ 200cm$^{-1}$ of the electromagnetic spectrum (Patel, 2015). The basic components of FTIR are given Figure 3.5.

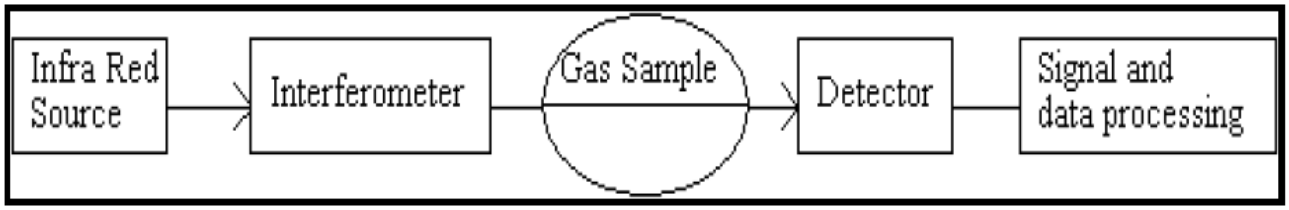


**Figure 3.5 Principal components of FTIR (Patel, 2015)**

The basic components of FTIR are:

- The source
- The interferometer
- The sample
- The detector

- The computer

As a source in FTIR, a glowing black body is used for emission of infrared energy. The energy of the produced light beam is controlled by an aperture and is further directed on the sample. Depending on the type of analysis, after entering into the sample compartment, the light beam is transmitted through surface of the sample. For final determination, the light beam ultimately enters into the detector. The detectors are designed in such a way that the signal of special interferogram is measured. After entering into the detector, the analyzed beam being digitized and furthered sent to the computer where the process of the Fourier transformation is done. The experimental setup of the FTIR is shown in Figure 3.6.

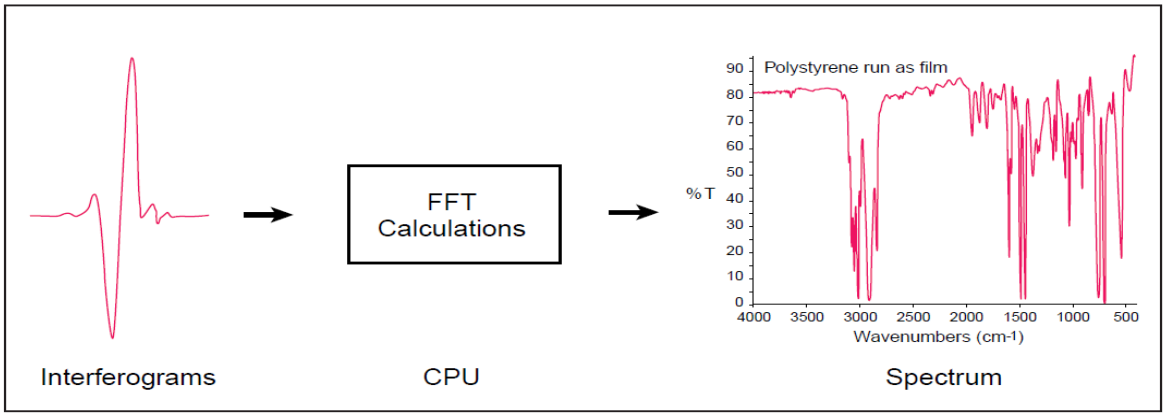


**Figure 3.6 Setup of FTIR (Patel, 2015)**

## 3.5 Instruments used for the study of phenol degradation

### 3.5.1 UV-Vis spectrophotometer

The degradation of phenol was analyzed by the UV-Vis spectrophotometer. With help of the UV-Vis spectrophotometer technique, phenol solution absorbance was measured before and after the degradation of phenol by $TiO_2$.

For the determination of absorbance or transmittance depending upon the wavelength of the electromagnetic radiation, spectrophotometer is used. The main components of the spectrophotometer are:

- A source
- A dispersion device

- A sample area
- Detectors

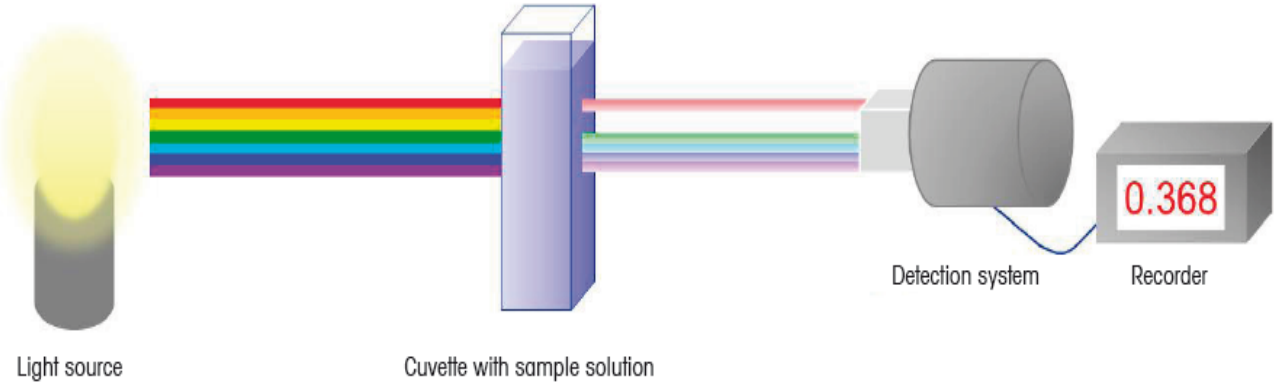


**Figure 3.7 Main components of UV-Vis Spectrophotometer (De Caro & Haller, 2015).**

Mainly two types of light sources are used in the spectrophotometer: first source of light is the deuterium arc lamp, which produces intensity in a continuous manner to the UV region and also produces intensity in the visible region and the tungsten lamp being the second source produces intensity over both of the UV and visible region. The dispersion device allows the light to get dispersed over the different wavelengths at different angles and at the end, the detector converts the light signal into the electrical signal (De Caro & Haller, 2015).

### 3.5.2 Principal of UV-Vis Spectrophotometer

Intensity of passing light through the placed sample in cuvette is measured by the UV-Vis spectrophotometer technique, and is compared with the prior intensity of light before entering into the sample. The spectrum of UV-Vis spectrophotometer is represented in the graphical form as absorbance which is the function of the wavelength.

### 3.5.3 Beer-Lambert law

When the light intensity passes through the sample, it is proportional to concentration of sample. With increase in sample concentration, intensity of light passing through the sample also increases. Hence, along with the length of the cuvette, as the length of the cuvette increases, the absorption of the light also increases. The equation describing the Beer-Lambert law is given as:

$$A = \varepsilon . c . d$$

Here, $c$ is concentration of sample in mol/L or g/L, $d$ the length of the cuvette is given in cm, $\varepsilon$ which the extinction coefficient is a sample constant and A is the absorbance (Caro, 2015; Braslavsky *et al*., 1988).

The UV-Vis spectrophotometer (SPECORD 200 PLUS) was used for the analysis of the phenol degradation. The degraded phenols were measured by the UV-Vis spectrophotometer apparatus at a wavelength of 500 nm.

### 3.6 Degradation efficiency

By using the values of difference in the absorption taken by the spectrophotometer, the efficiency of the degradation can be determined by the given equation (Chiu *et al*., 2019):

$$\text{Degradation Efficiency (\%)} = \frac{C_0 - C}{C_0} \times 100$$

$C_0$ is concentration of solution at t=0 and,

C is concentration of solution after some irradiation time.

### 3.7 Photocatalytic experiments

#### 3.7.1 Experimental Setup

Degradation of the phenol was done under the irradiation of UV (8W) and Visible (18W) light with varying the quantity of both visible and UV light. The degradation was done under different time intervals for the period of 6 h and various samples were taken out at the various time intervals. Both the experiments of UV and Visible light were run side by side in various compartments of the photocatalytic chamber. Precisely, 50 mg $L^{-1}$ of the phenol solution was taken with the calculated quantity of the dye sensitized nanoparticles. The phenol solution was irradiated for the time period of 6 h using both UV light and visible light. Experimental setup for degradation of phenol by the dye sensitized nanoparticles is shown in Figure 5.

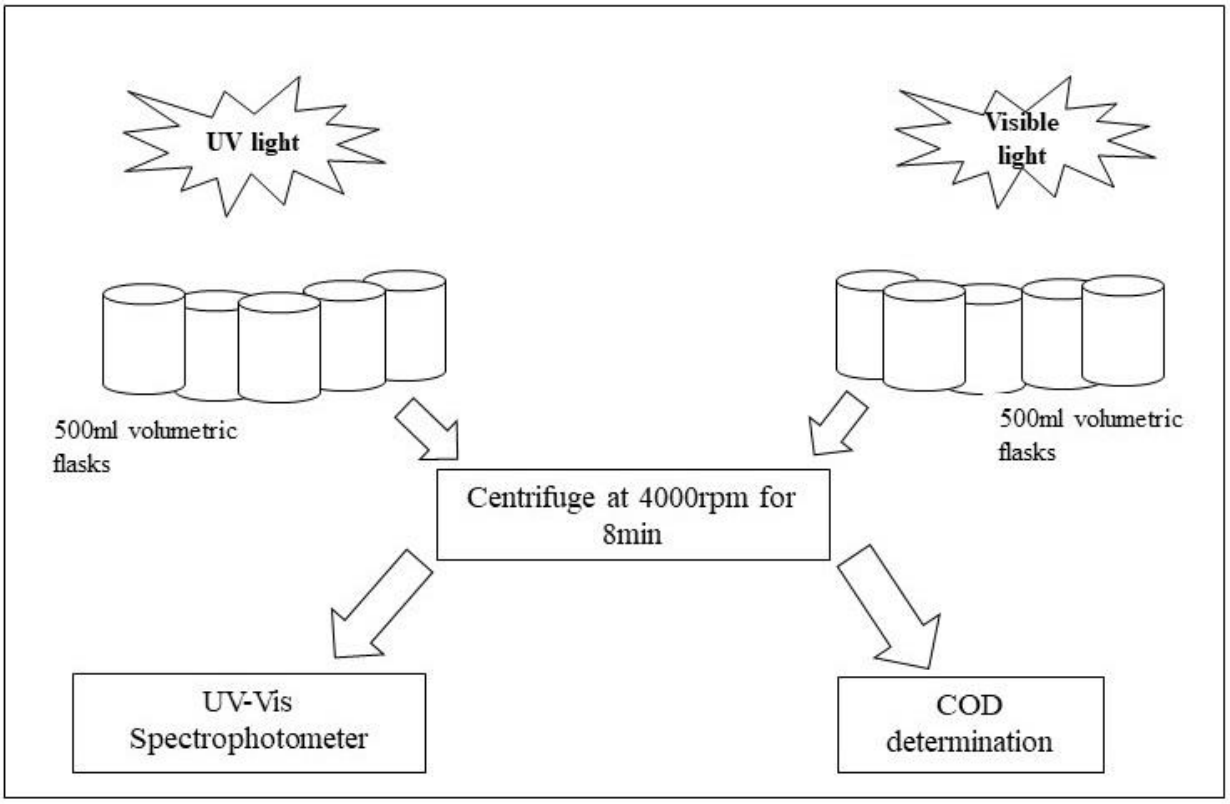


**Figure 5: Setup for degradation of phenol**

### 3.8. Preparation of solution

Five different volumetric flasks were taken and in each of the flask 50 mg/L of phenol solution was prepared by adding 250 mg phenol in 500 mL of volumetric flask and filled volume up to the mark by adding distilled water. After preparing the phenol solution, different quantities of dye sensitized $TiO_2$ nanoparticles were added in solution of phenol in order to find out optimum dosage of dye sensitized $TiO_2$ nanoparticles for degradation of phenol. Then, volumetric flasks were placed on the magnetic stirrer for 5 min for the mixing of phenol and nanoparticles (Chowdhury *et al*., 2012). Samples were withdrawn at different time periods, and the concentration of phenol was analyzed by 4-aminoantipyrene method (Varadaraju *et al*., 2018) with UV-Vis spectrophotometer at 500 nm wavelength and COD was also determined.

# 4 RESULTS AND DISCUSSION

## 4.1 XRD Analysis

XRD analysis of nanoparticles was carried out to determine their polymorph phase, crystallinity and their composition. XRD graphs were attained by powder XRD technique using Cu-Kα radiation = 1.5418 Å at an angle of 2θ from 10° to 80° (Bunaciu *et al*., 2015). Figure  shows the XRD results of pure $TiO_2$ nanoparticles where 2θ peaks at 25.56°, 37.96°, 48.2°, 54.04° and 55.2° are visible. The presence of different peaks at 2θ values of 25.5°, 37.9°, 48.2° and 55.2° shows that $TiO_2$ nanoparticles mainly consists of anatase phase. All these peaks showed that titania nanoparticles were highly crystalline in nature and were upto 80% anatase.

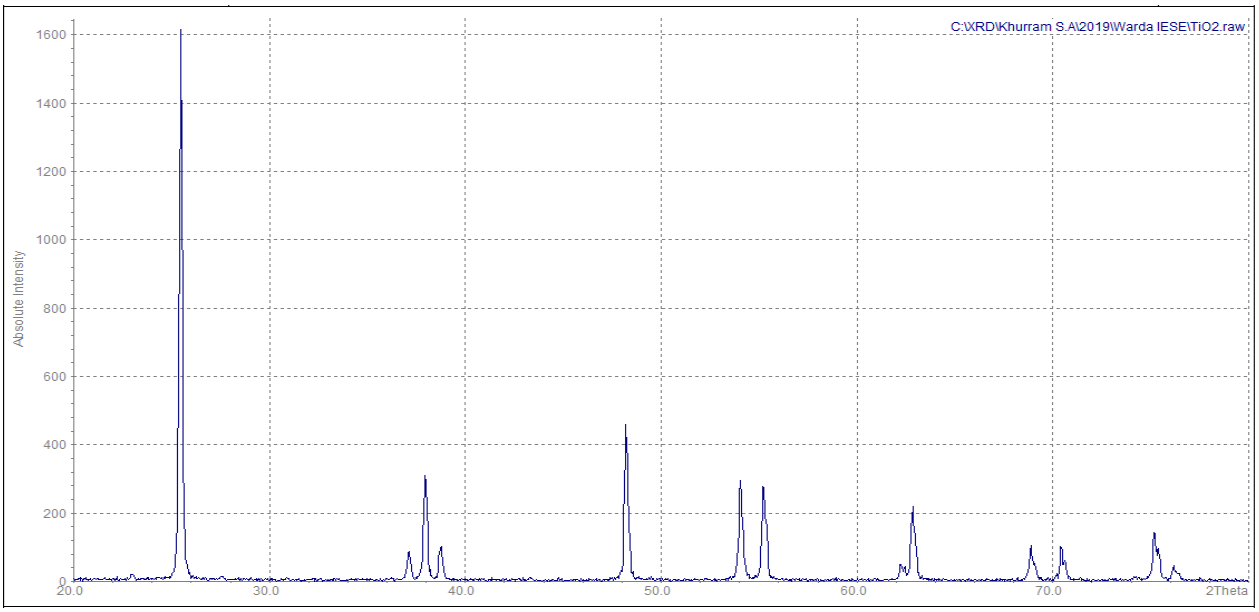


**Figure 4.1: XRD intensity plot fore pure titania nanoparticles**

Figure 4.2 displays the XRD graph of dye sensitized nanoparticles with concentration of 1x $10^{-2}$ mM. The diffraction peaks at 2θ = 25.56°, 38.16°, 48.32° and 55.24° shows the anatase crystalline phase of the dye sensitized nanoparticle. The first peak of concentration 1x $10^{-2}$ mM appears at 2θ value of 25.56°. The crystalline nature of these dye sensitized nanoparticles resulted primarily due to calcination of pure $TiO_2$ nanoparticles at 550$^o$ C for 6 hrs.

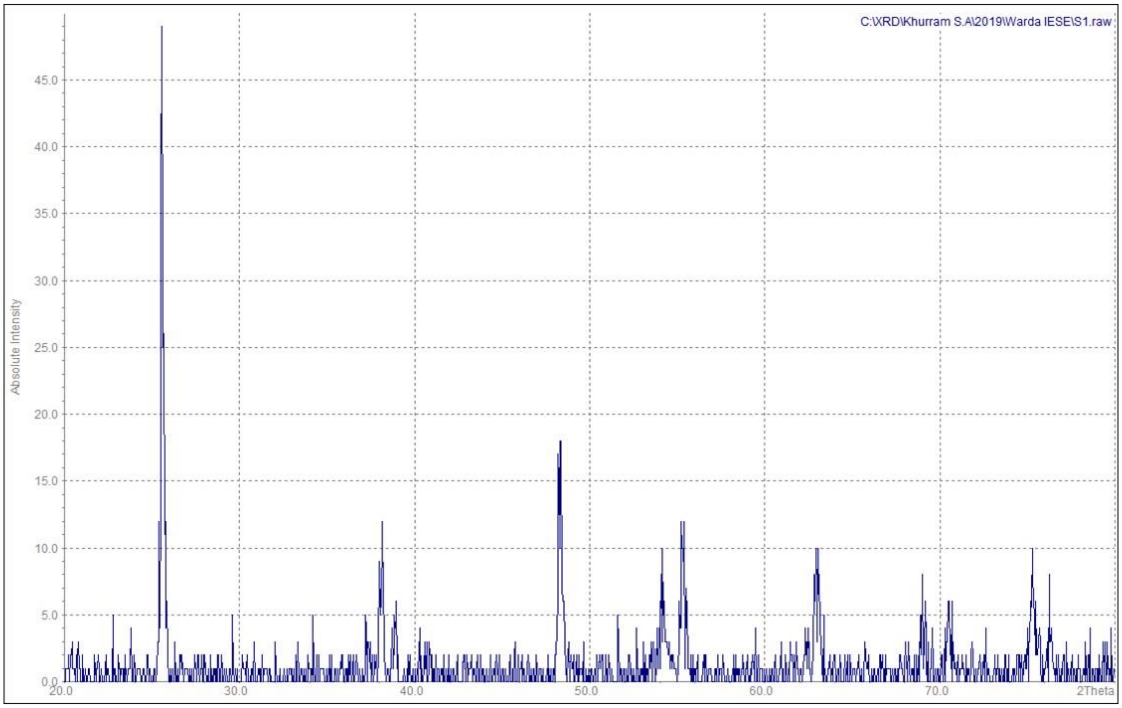


**Figure 4.2: XRD intensity plot for concentration $1x10^{-2}$ mM dye sensitized nanoparticles**

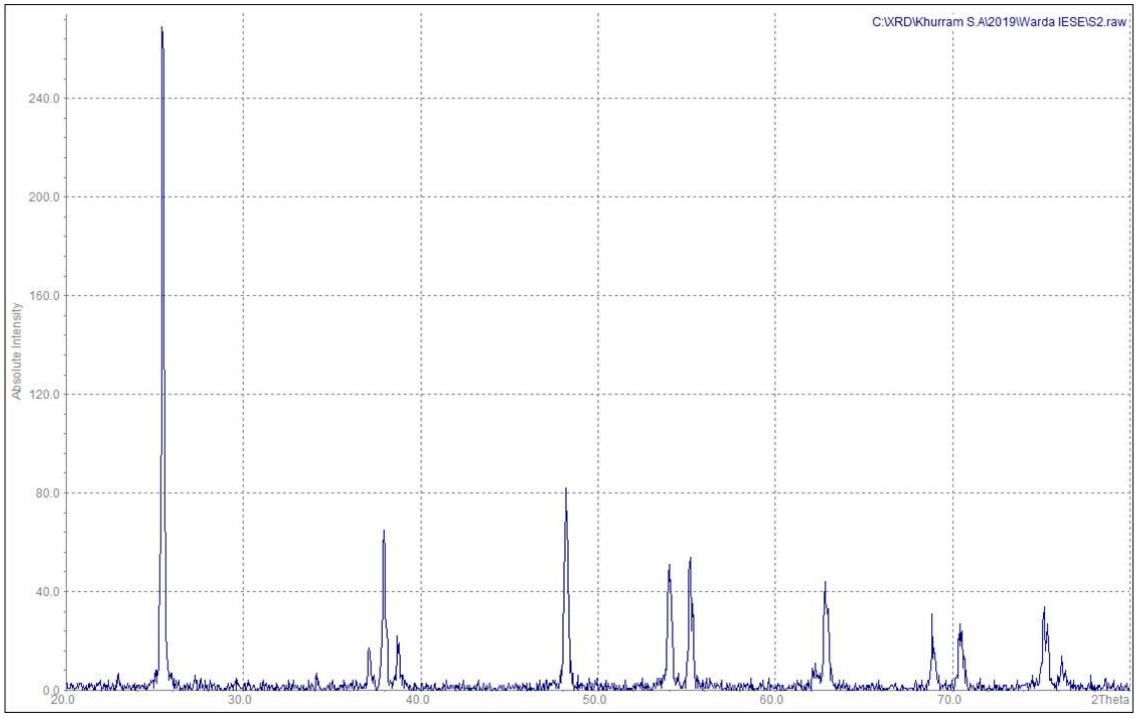


**Figure 4.3: XRD intensity for concentration $2x10^{-2}$ mM dye sensitized nanoparticles**

Figure 4.3 displays the XRD graph of dye sensitized nanoparticles having the concentration of $2x10^{-2}$ mM with peaks appearing at 25.4°, 37.92°, 48.2° and 55.2°. The highest peak at 25.52° represented the anatase phase. These peaks represented the crystallinity and purity of the dye sensitized nanoparticles.

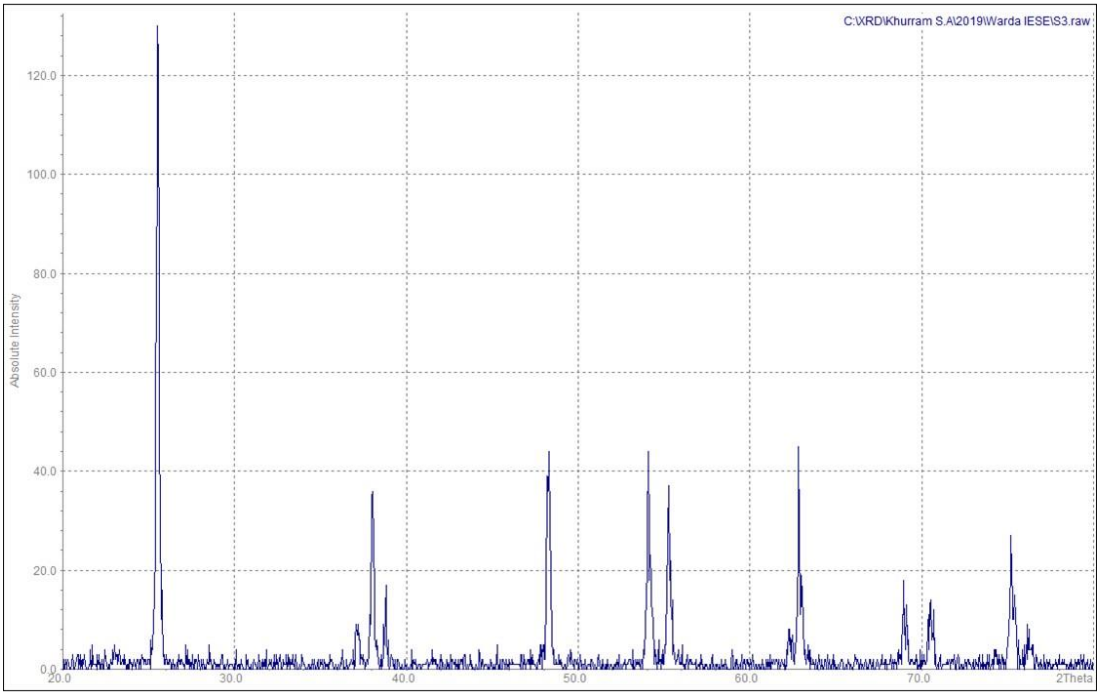


**Figure 4.4: XRD intensity plot for concentration $3x10^{-2}$ mM dye sensitized nanoparticles**

Figure 4.4 shows the different peaks at 2θ for the concentration of $3x10^{-2}$ mM of the dye sensitized nanoparticles. The peaks at 25.52°, 38.04°, 48.32° and 55.28° represented the crystalline nature of dye sensitized nanoparticles. The anatase phase resulted when the temperature appeared between 300-500°C.

Figure 4.5 shows the XRD pattern of concentration $4x10^{-2}$ mM of the dye sensitized nanoparticles. The peaks show 2θ at 25.32°, 37.76°, 48.04° and 55.04°. Anatase phase shows high photoconductivity performance as compared to the rutile phase because of the difference in energy of band gap of anatase and rutile phase which is ~ 3.2eV and ~3.0eV, respectively (Hanaor & Sorrell, 2011). Figure 4.6 shows the XRD graph of the concentration of $5x10^{-2}$ mM.

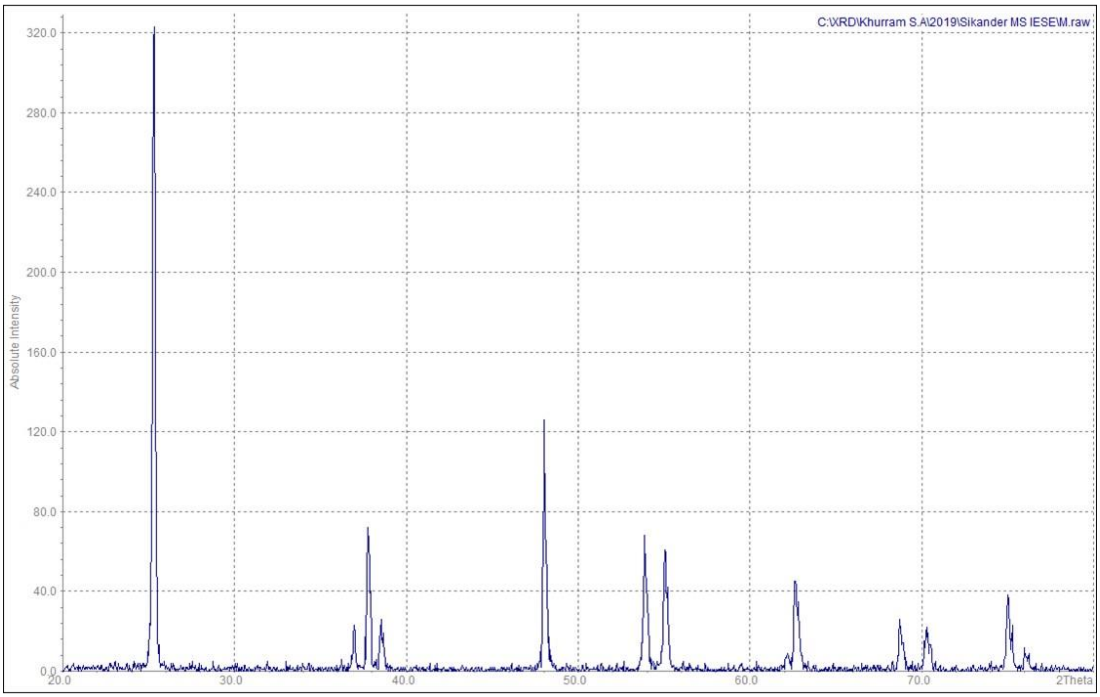


**Figure 4.5: XRD intensity plot for concentration $4x10^{-2}$ mM dye sensitized nanoparticles**

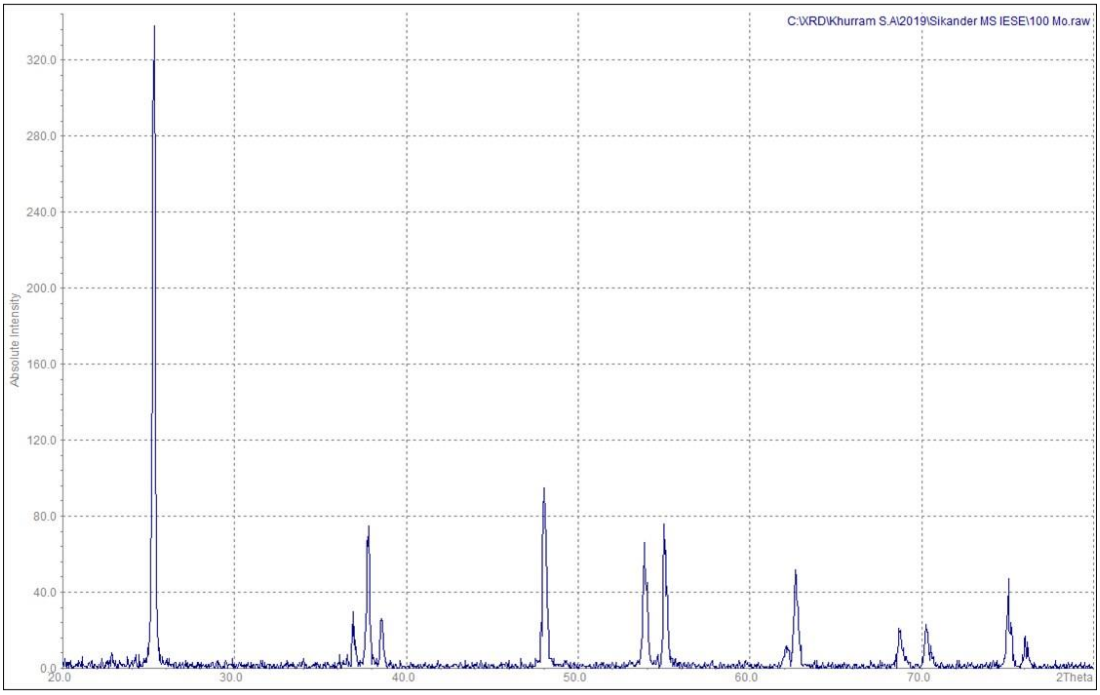


**Figure 4.6: XRD intensity plot for concentration $5x10^{-2}$ mM dye sensitized nanoparticles**

## 4.2 SEM Analysis

Morphology and diameter of prepared $TiO_2$ nanoparticles were considered under the SEM. The SEM images showed the porous, sponge-like structure of high porosity and roughness. The SEM images of both pure $TiO_2$ nanoparticles and the dye sensitized nanoparticles were taken by JEOL JSM- 6490A at an acceleration voltage of 20kV. Figure 4.7 shows SEM image of pure $TiO_2$ nanoparticles under the magnification at X50,000. The diameter of the spherical $TiO_2$ nanoparticles ranged from 20-60 nm.

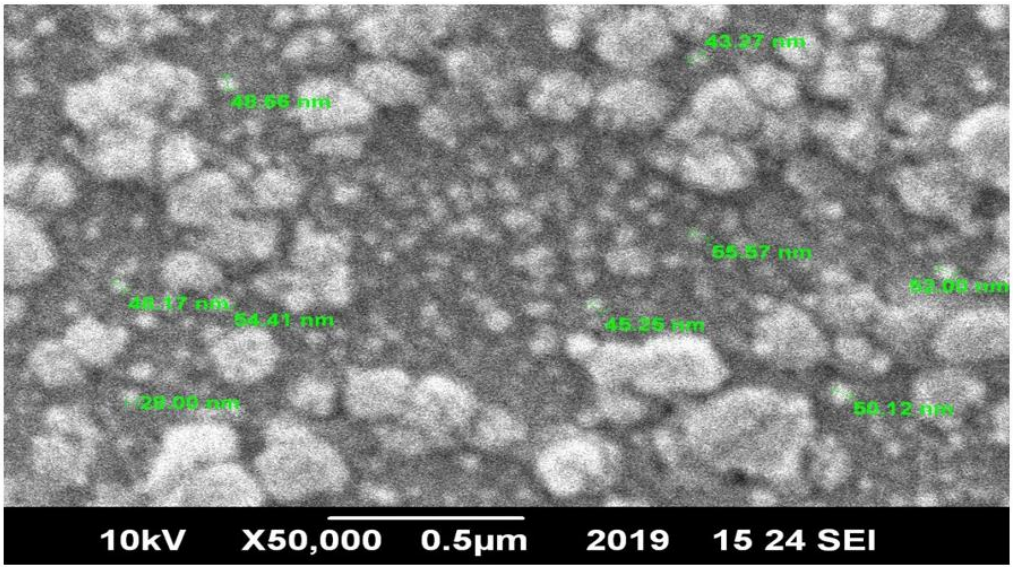


**Figure 4.7: SEM image of pure titania nanoparticles at X50,000**

Figures 4.8 and 4.9 show SEM image of concentrations $1x10^{-2}$ mM and $2x10^{-2}$ mM of the dye sensitized nanoparticles under the magnification of X40,000 and X45,000, respectively. The SEM images of the dye sensitized nanoparticles seemed to be rougher and complex showing high area of surface for the dye adsorption on $TiO_2$ nanoparticles.

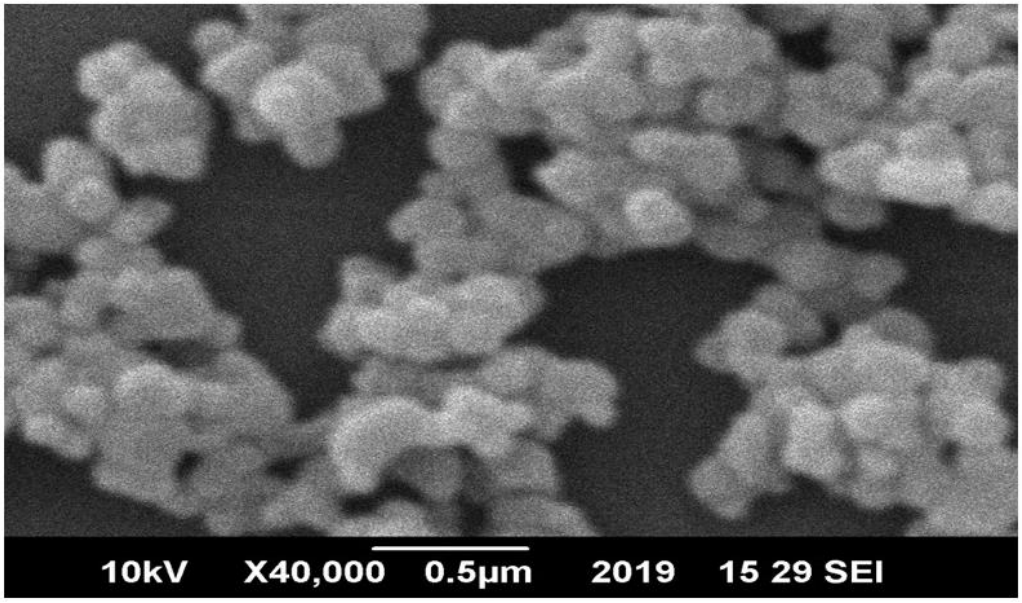


**Figure 4.8: SEM image of concentration $1x10^{-2}$ mM dye sensitized nanoparticles**

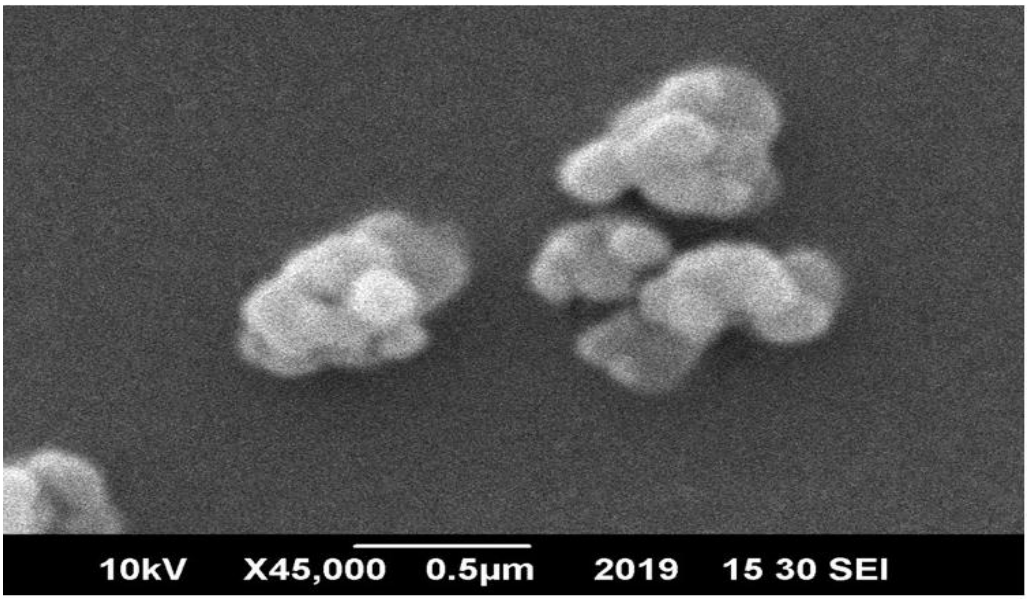


**Figure 4.9: SEM image of concentration $2x10^{-2}$ mM dye sensitized nanoparticles**

Figures 4.10, 4.11 and 4.12 show the SEM images of the concentration $3x10^{-2}$ mM, $4x10^{-2}$ mM, and $5x10^{-2}$ mM, respectively of dye sensitized nanoparticles under the magnification of X40,000. The SEM images of the dye sensitized nanoparticles showed the diameter at various concentrations in the range of 30-70nm. The SEM images showed the high complexity of the nanoparticles with high adsorption capacity for the dye molecules. The SEM images showed that the morphology of

the dye sensitized is more rough, porous and sponge-like giving high roughness and complexity to structure of nanoparticles.

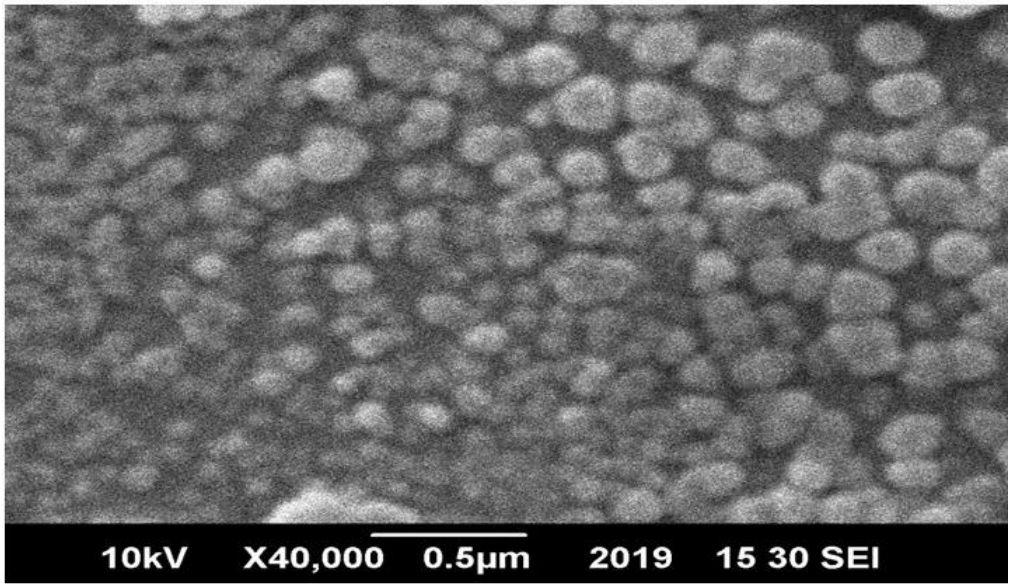


**Figure 4.10: SEM image of concentration $3x10^{-2}$ mM dye sensitized nanoparticles**

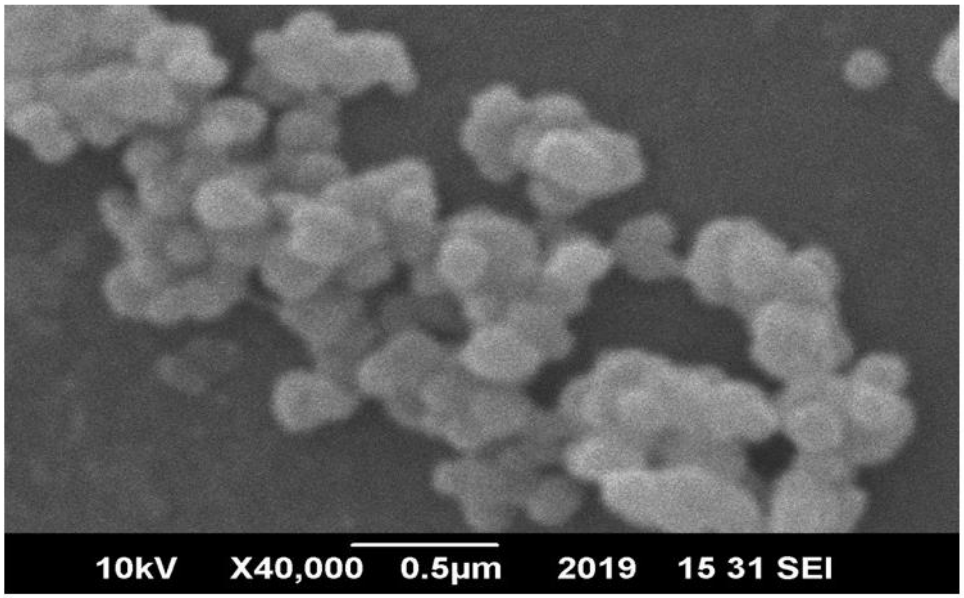


**Figure 4.11: SEM image of concentration $4x10^{-2}$ mM dye sensitized nanoparticles**

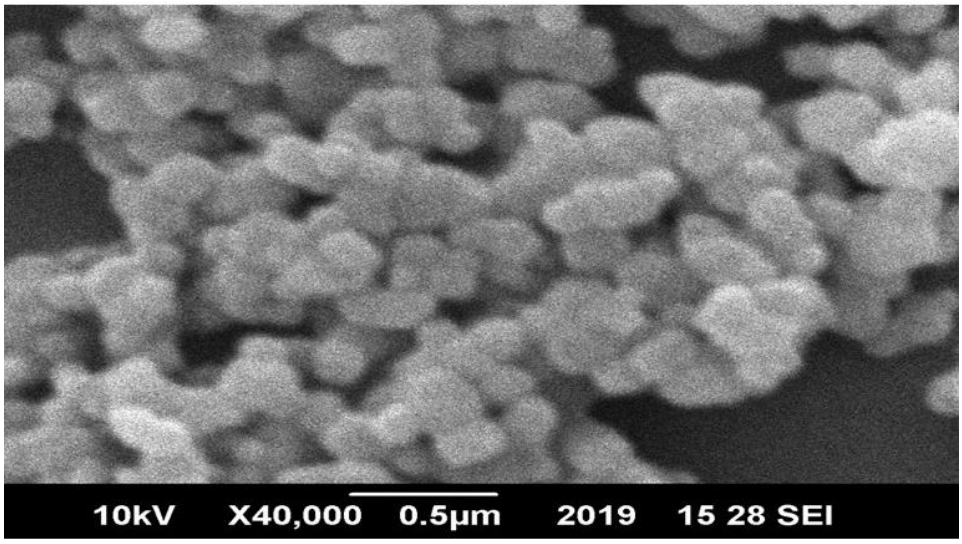


**Figure 4.12: SEM image of concentration $5x10^{-2}$ mM dye sensitized nanoparticles**

### 4.3 FTIR Analysis

Fourier Transform Infrared Spectroscopy (FTIR) technique was conducted for studying and comparing the various functional groups present in pure $TiO_2$ nanoparticles and in the dye sensitized $TiO_2$ nanoparticles. FTIR spectra of these nanoparticles governed by an intensive and broad band from 3000-3500 $cm^{-1}$ showing the stretching vibrations of hydroxyl group ($OH^-$) that are either symmetric or asymmetric of the water molecules present in the structure of the nanoparticles (Khan *et al*., 2018).

Figure 4.13 displays FTIR spectra for pure $TiO_2$ nanoparticles. In case of pure $TiO_2$ nanoparticles, band at 3401.75 $cm^{-1}$ assigned to the water of hydration existing in the solution, while the band at 2916.01 $cm^{-1}$ showed asymmetric vibrations of $–CH_3$ groups. The third band at 1630 $cm^{-1}$ showed the bending modes of water assigned as Ti-OH.

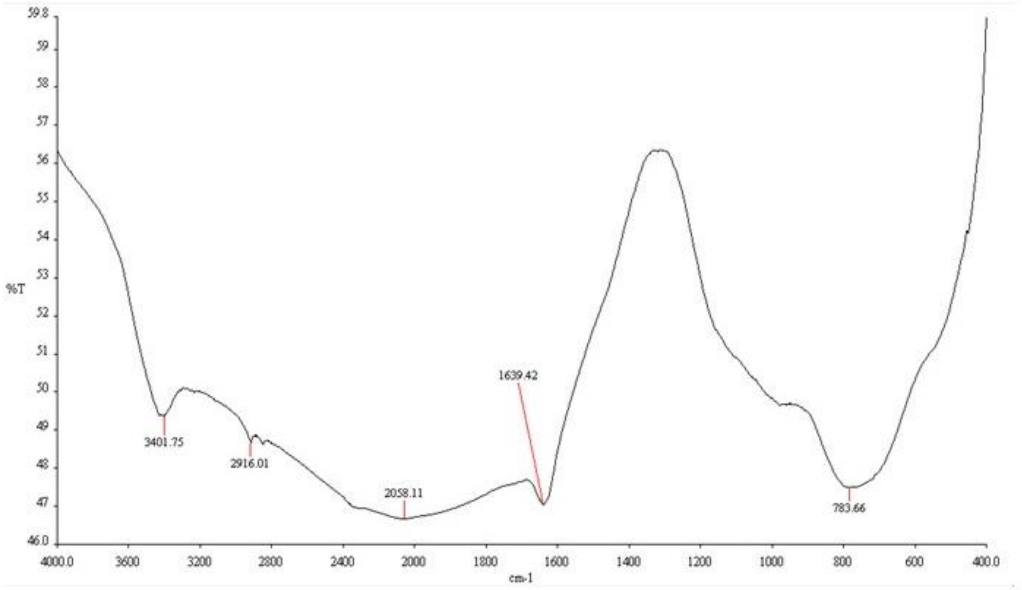


**Figure 4.13: FTIR spectrum of pure $TiO_2$ nanoparticles**

Figures 4.14 and 4.15 show FTIR spectra of the dye sensitized nanoparticles with concentration of $1x10^{-2}$ mM and $2x10^{-2}$ mM, respectively. The first band in both of the concentrations at 3400 $cm^{-1}$ shows the stretching vibration of O-H group. While 2852.85 $cm^{-1}$ and 2915.59 $cm^{-1}$, the asymmetric vibration of $–CH_3$ group was exhibited. The band ranging from 2260-2100 $cm^{-1}$ showed variable stretching of C≡C group.

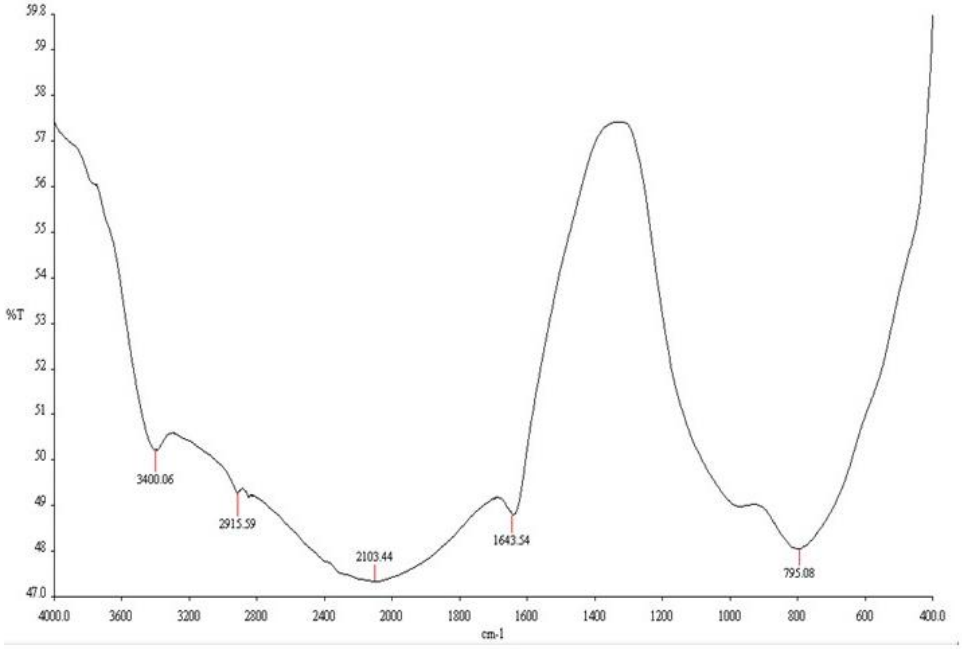


**Figure 4.14: FTIR spectrum of concentration $1x10^{-2}$ mM dye sensitized nanoparticles**

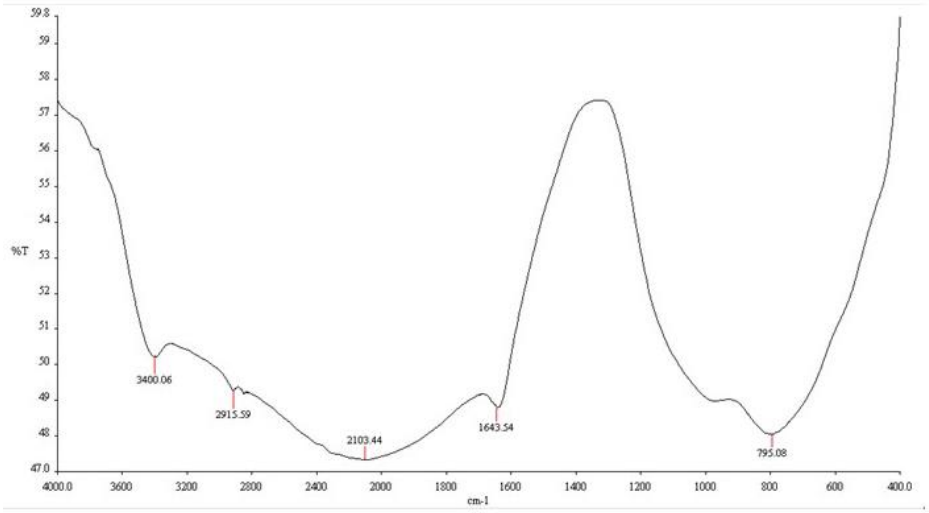


**Figure 4.15: FTIR spectrum of concentration $2x10^{-2}$ mM dye sensitized nanoparticles**

Figures 4.16 and 4.17 show FTIR spectra of the dye sensitized nanoparticles with concentrations $3x10^{-2}$ mM and $4x10^{-2}$ mM, respectively. The first band ranging from 3300-3400 $cm^{-1}$ showed presence of N-H group in structure of dye sensitized nanoparticles. Presence of such N-H group confirmed presence of safranin adsorbed on the $TiO_2$ nanoparticles as the functional group was a part of the molecular structure of the safranin dye. The FTIR spectral band at 2921.84 $cm^{-1}$ and at

2848.80 $cm^{-1}$ indicated the presence of $–CH_3$ group. The band ranging from 1640-1660 $cm^{-1}$ was attributed to presence of C=C group.

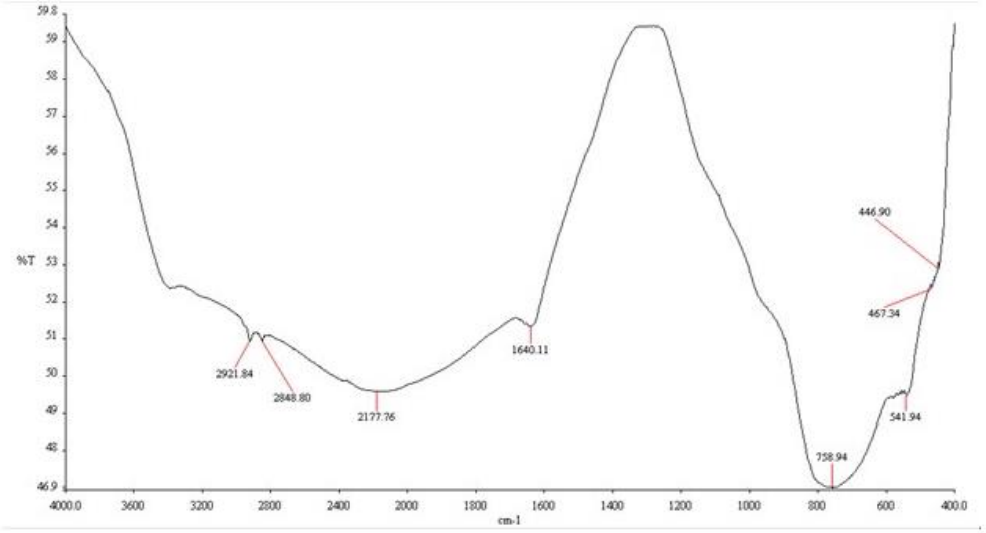


**Figure 4.16: FTIR spectrum of concentration $3x10^{-2}$mM dye sensitized nanoparticles**

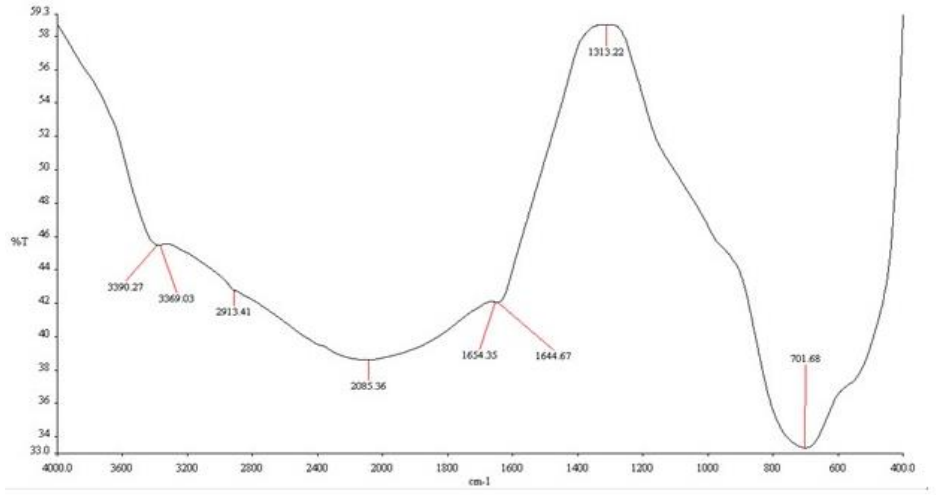


**Figure 4.17: FTIR spectrum of concentration $4x10^{-2}$mM dye sensitized nanoparticles**

## 4.4 UV spectrum for initial dye absorbance

For the calculation of initial dye absorbance on the surface of $TiO_2$ nanoparticles, a standard curve of different standards of safranin dye was prepared. Standards of safranin solution ranging from $1x10^{-2}$ mM to $5x10^{-2}$ mM were prepared and measured at wavelength of 516 nm at the UV-spectrophotometer. Figure 4.18 shows the standard curve of the different prepared standards of

safranin solutions. In figure 4.19, as shown concentrations of safranin dye increased in the solution, the level of absorbance in the UV- spectrophotometer increased.

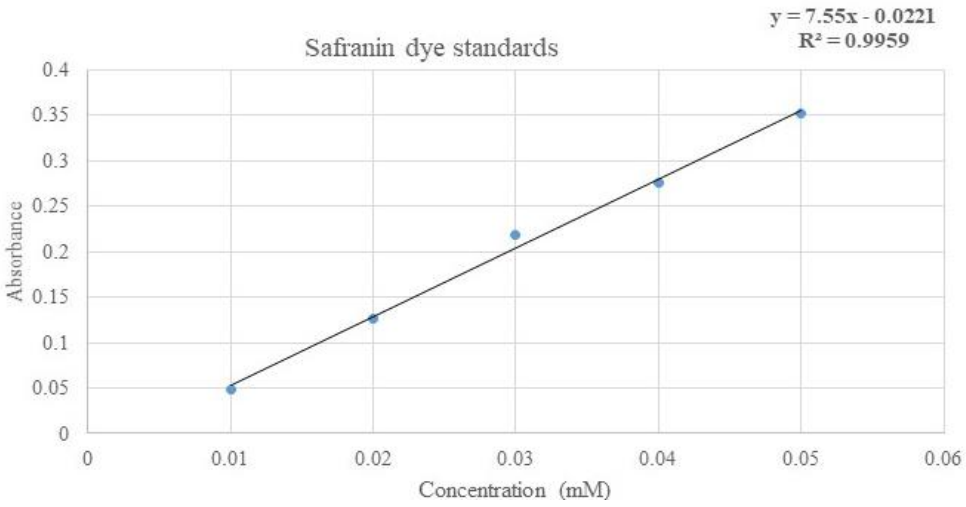


**Figure 4.18: Calibration curve of safranin solution ranging from $1x10^{-2}$ mM to $5x10^{-2}$ mM**

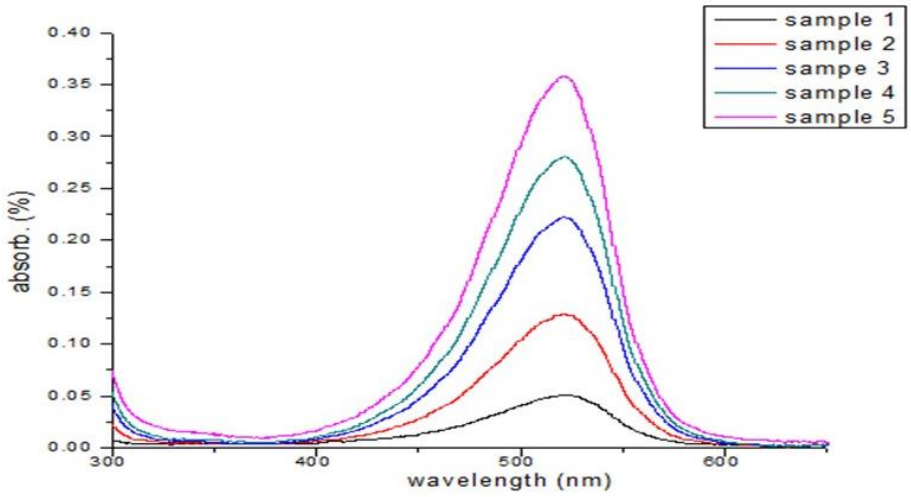


**Figure 4.19: Curve for initial absorbance of safranin dye solution ranging from $1x10^{-2}$ mM to $5x10^{-2}$ mM**

After calculating the curve of initial absorbance of safranin solutions from $1x10^{-2}$ mM to $5x10^{-2}$ mM, it was obvious that with the increasing concentration of the safranin dye, the absorbance of dye increased according to the Beer-Lambert law. By calculations of initial absorbance of the various solutions of the safranin dye, the final absorbance of these solutions on the added dosage of $TiO_2$ nanoparticles (TNPs) were measured at wavelength of 516 nm at the UV-

spectrophotometer by separating TNPs from the dye solution by the process of centrifugation and filtration. After having the values of initial and final absorbance measured at the UV-spectrophotometer, dye adsorbed per gram of TNPs and the percentage (%) of dye adsorbed on the TNPs were calculated and on the basis of calculations the concentration of $4x10^{-2}$ mM was taken as the optimum concentration of safranin solution due to the fact that 70.85% of the safranin dye was adsorbed on the TNPs which was maximum in comparison to the other concentrations. Table 4.1 illustrates the various calculations done for the purpose of the optimum dosage.

**Table 4.1: Determination of optimum concentration of safranin solution**

| **Initial Concentration** | | **Initial Absorbance** | **Final Absorbance** | **Final Concentration** | | **Dye Absorbed per g** | **% of Dye Adsorbed** |
|---|---|---|---|---|---|---|---|
| **(mM)** | **(mg)** | **(AU)** | **(AU)** | **(mg)** | **(mM)** | **(mg)** | **%** |
| 0.01 | 3.508 | 0.049 | 0.032 | 2.51 | $7.16x10^{-3}$ | 0.995 | 28.3 |
| 0.02 | 7.016 | 0.127 | 0.037 | 2.74 | $7.82x10^{-3}$ | 4.276 | 60.9 |
| 0.03 | 10.524 | 0.218 | 0.051 | 3.39 | $9.68x10^{-3}$ | 7.128 | 67.73 |
| 0.04 | 14.032 | 0.276 | 0.066 | 4.09 | 0.011 | 9.942 | 70.85 |
| 0.05 | 17.54 | 0.35 | 0.14 | 7.48 | 0.021 | 10.082 | 57.4 |

As shown in table, optimum concentration of $4x10^{-2}$ mM was further used in the degradation experiments.

## 4.5 Effect of parameters

### 4.5.1 Optimizing catalyst concentration

The comparative study for the optimization of initial concentration of catalyst was done. Different concentrations of the catalyst loading were taken for degradation of phenol and rate of phenol degradation with different time periods i.e., 0, 1, 2, 4 and 6 h were measured. Figure 4.20, 4.21, 4.22 and 4.23 show the degradation of phenol with catalyst dosages of 125 mg/500mL, 250 mg/500mL, 500 mg/500mL and 1000 mg/500mL, respectively with different time intervals.

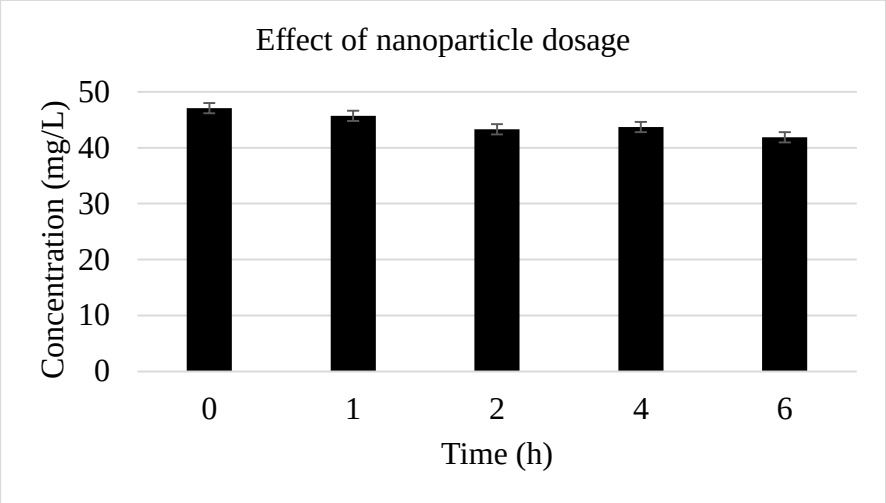


**Figure 4.20: Effect of 125 mg/500mL dosage on phenol degradation**

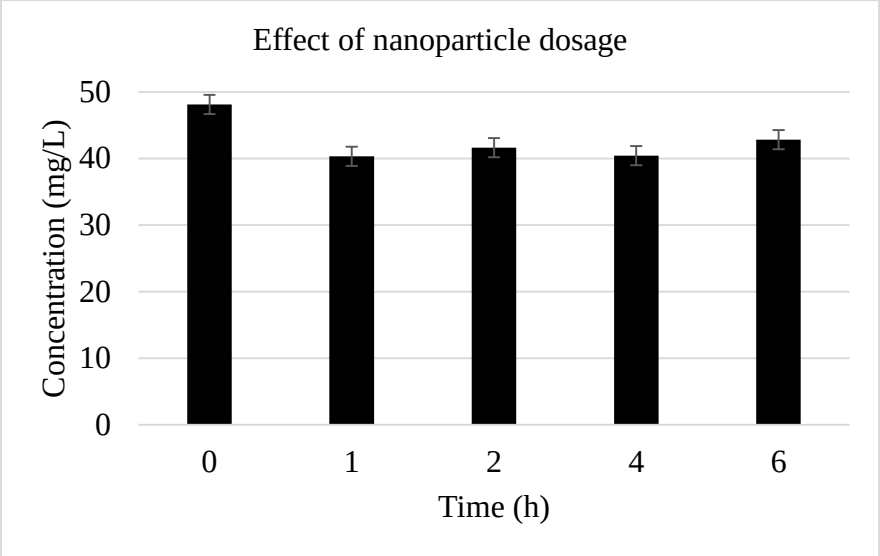


**Figure 4.21: Effect of 250 mg/500mL dosage on phenol degradation**

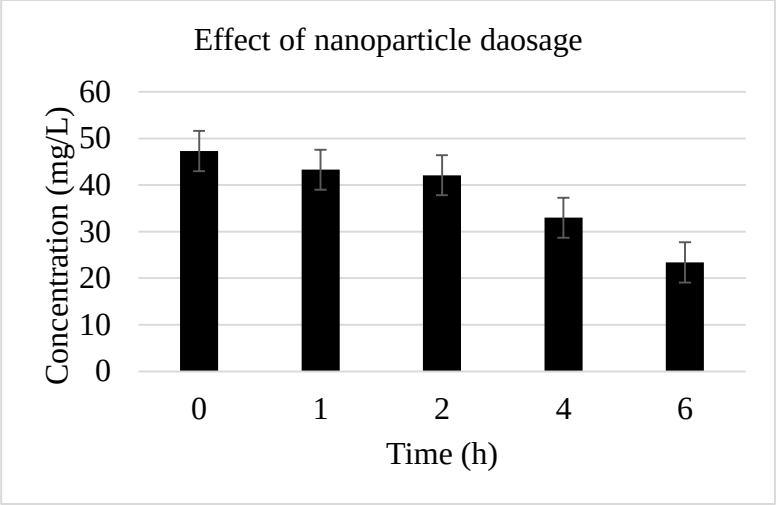


**Figure 4.22: Effect of 500 mg/500mL dosage on phenol degradation**

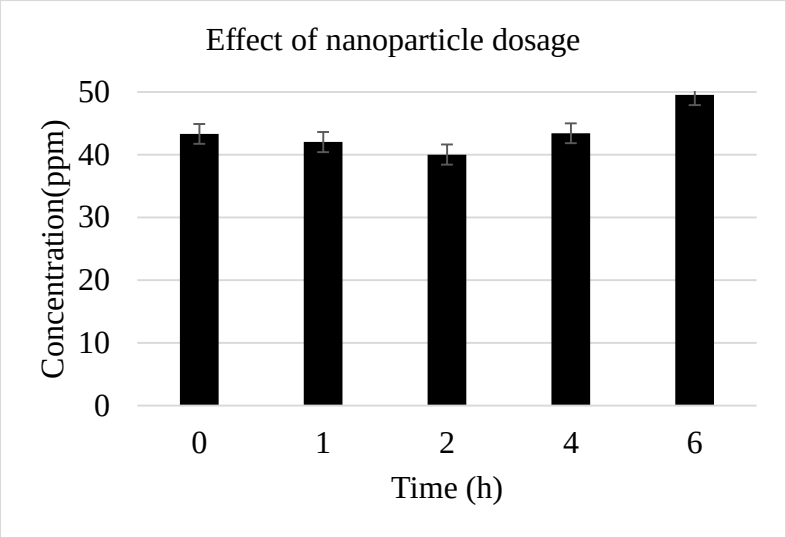


**Figure 4.23: Effect of 1000 mg/500mL dosage on phenol degradation**

As shown in the above graphs, the effect of dye sensitized TNPs on the phenol degradation were determined. It was found that initially with the increase in catalyst dosage, the rate of degradation should increase. But after a certain point, it was found that with further increase in catalyst concentration, no prominent degradation in phenol concentration was found. It might be due to that, with increase in catalyst concentration, light penetration decreased owing to the increase in turbidity due to the increased concentration in catalyst dosage (Choquette-Labbe *et al*., 2014). It

was concluded that 500 mg of nanoparticles were taken to be the optimum dosage. In all cases, the concentration of 50 mg/L of phenol solution was taken for the degradation study.

### 4.5.2 Effect of light intensity

Band gap energy of $TiO_2$ was 3.2 eV that is usually activated by the ultraviolet region of light. But the modification of dye sensitization lowers the band gap energy of $TiO_2$ so that the electrons should get excited even under the visible region of light. From the literature, it is confirmed that the process of dye sensitization activates $TiO_2$ in the visible region from 420 to 800 nm (Zangeneh *et al*., 2015). So, to confirm the fact that dye sensitization activates $TiO_2$ in region of visible light, the experiments of degradation of phenol by dye sensitized nanoparticles were carried out both in the visible and ultraviolet region.

Two different intensities of ultraviolet light (8W & 16W) and visible light (18W & 36W) were used in the research to analyze impact of both light on degradation of 50 mg/L of phenol by the dye sensitized nanoparticles. Figures 4.24 and 4.25 show the impact of both 8W and 16W (UV light) intensities, respectively for the phenol degradation.

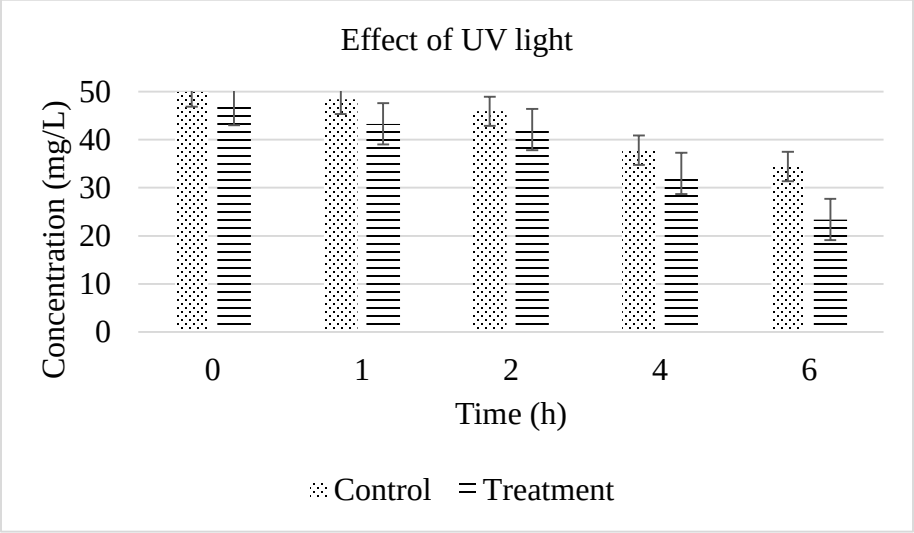


**Figure 4.24: Effect of 8W UV light on phenol degradation**

The control only contained 50 mg/L of phenol solution with no added dye sensitized TNPs, while the treatment contained the optimum dosage that was 500 mg/500mL of the dye sensitized TNPs in the 50 mg/L of phenol solution. Figure 4.25 shows the impact of 16W intensity of UV light on phenol degradation.

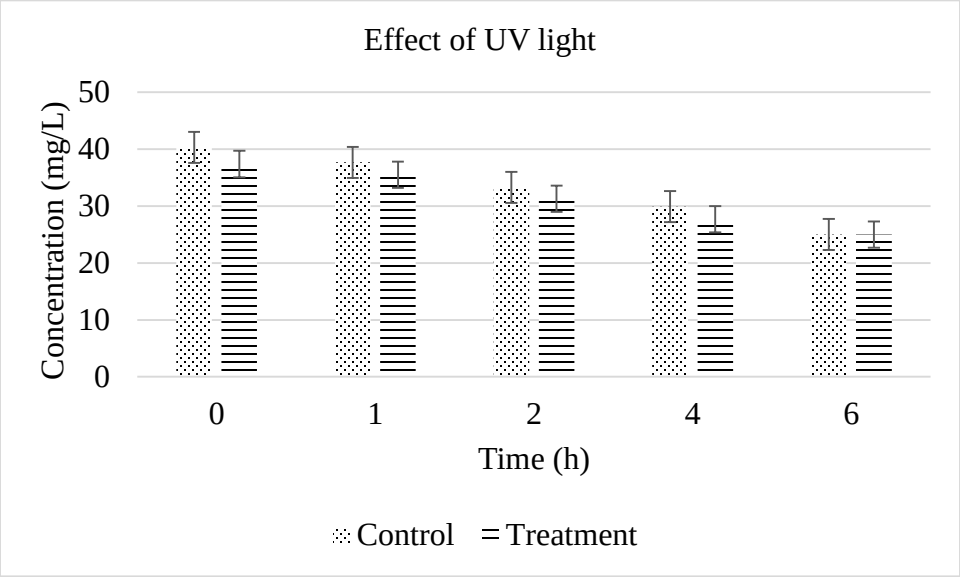


**Figure 4.25: Effect of 16W UV light on phenol degradation**

As obvious from the results shown above, there was no such prominent phenol degradation using UV light because under UV light, there was no such activation of dye sensitized TNPs. However, UV light of high intensity that was 16W, the 50 mg/L concentration of phenol was lowered to 25 mg/L at time interval of 6 h. Wang *et al*. (2017) reported that under UV light lamps of 24W

intensity, $TiO_2$ nanoparticles degraded 72.4% of 100 mg/L phenol in 3 h. Figures 4.26 and 4.27 show the effect of visible light with intensities 18W and 36W, respectively.

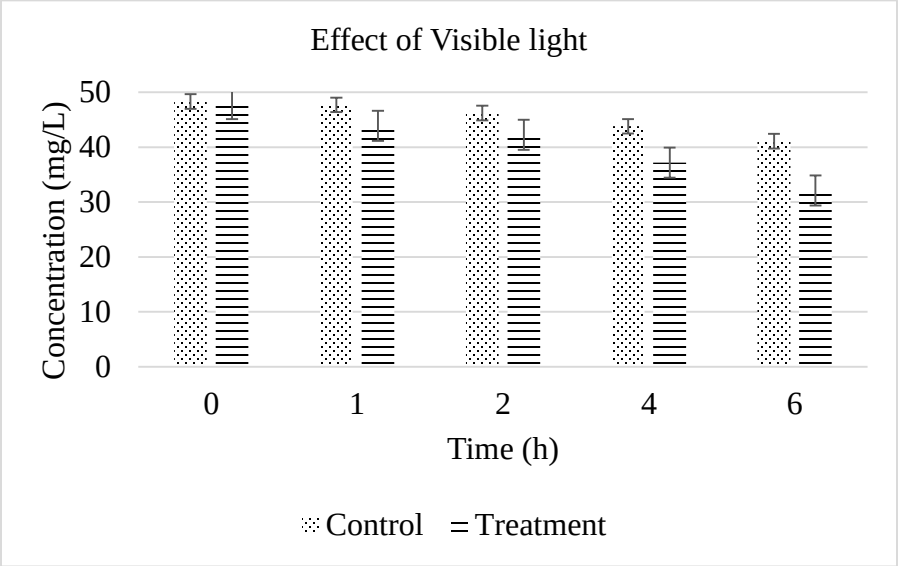


**Figure 4.26: Effect of 18W visible light on phenol degradation**

The effect of visible light with two different intensities (18W & 36W) over a time period starting from 0 to 6 h was determined. As the time period increased, rate of degradation of phenol by dye sensitized TNPs increased.

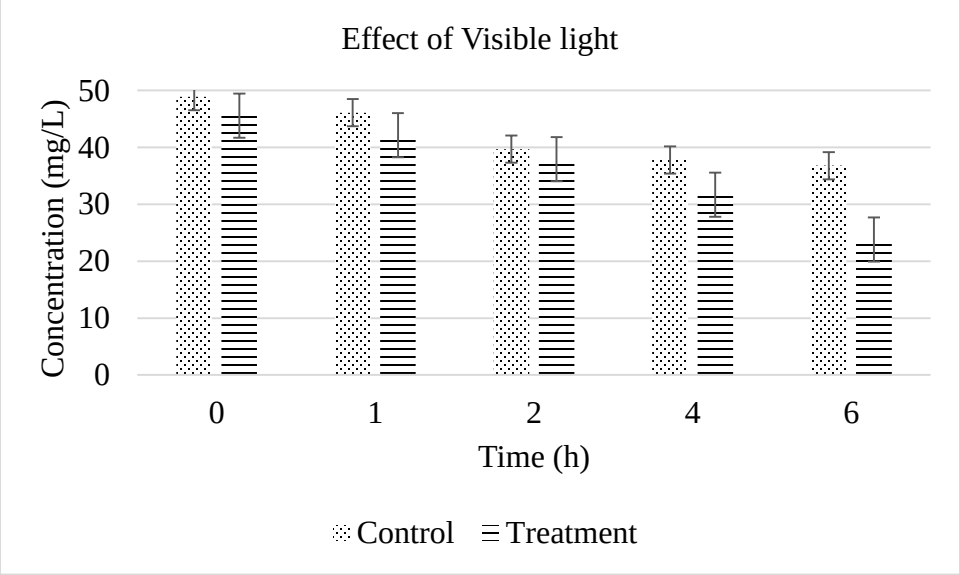


**Figure 4.27: Effect of 36W visible light on phenol degradation**

As reported in literature by Haghighatzadeh in 2020, curcumin sensitized $TiO_2$ nanoparticles degraded phenol to only 52 % in time period of 6 h under 150W of visible light. Under visible light with high intensity, which was 36W, the phenol degradation was 54% after period of 6 h, as under visible light the dye sensitized TNPs get excited which help in the degradation of 50 mg/L of phenol solution. Reason of degradation of phenol up to only 54% might be due to less exposure that was only for 6 h under low visible light intensity (36W). Gosh *et al*. (2020) reported that under visible light intensity of 60 mW $cm^{-2}$ mango steel sensitized $TiO_2$ nanoparticles were able to degrade methylene blue to 78% within time period of 2 h.

### 4.5.3 Effect of pH

Photocatalytic degradation of phenol by 500 mg/mL dosage of dye sensitized nanoparticles was carried out at acidic pH of 3. The effect of pH was determined at the highest optimized intensities of both UV (16W) and visible light (36W) because at both intensities the degradation of phenol was observed to be high.

As reported in literature by Chowdhury *et al*. (2012), at acidic pH, the point of charge of $TiO_2$ becomes positive, and safranin dye is a basic dye having positive charge, so at low pH the adsorption of dye becomes difficult and the rate of degradation of phenol decreases. At basic pH, point of charge of $TiO_2$ becomes negative, the dye being positively charged, strongly gets adsorbed on the surface of $TiO_2$ and the rate of degradation increases due to the dye sensitization of $TiO_2$.

Figure 4.28 displays the effect of acidic pH 3 under 16W of UV light for the degradation of phenol, whereas Figure 4.29 shows the degradation of phenol at acidic pH of 3 under 36W of visible light at different time intervals.

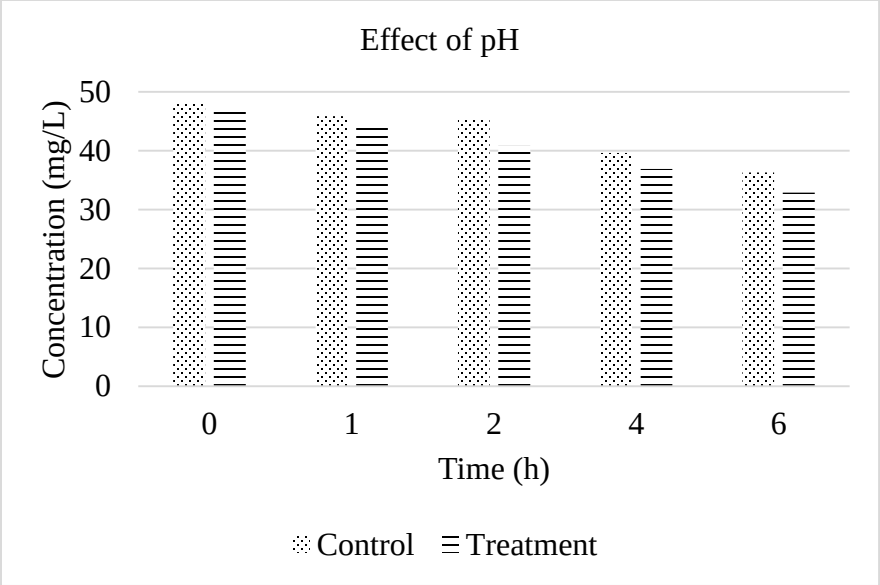


**Figure 4.28: Effect of pH 3 under 16W UV light on phenol degradation by dye sensitized TNPs**

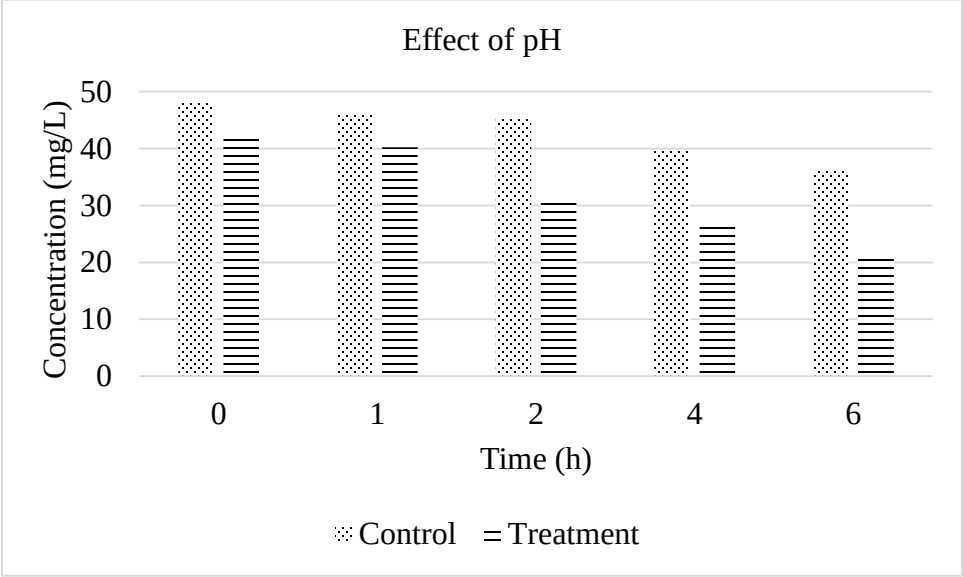


**Figure 4.29: Effect of pH 3 under 36W visible light on phenol degradation by dye sensitized TNPs**

The degradation rate of phenol by dye sensitized TNPs was lower due to less adsorption of dye on $TiO_2$ nanoparticles but the rate of degradation could be easily increased at basic pH due to the fact that the positively charged dye would be strongly adsorbed on the negatively charged $TiO_2$

nanoparticles. However, under visible light intensity of 36W the concentration of phenol was decreased to 20.9 mg/L from 50mg/L in comparison to 32.1 mg/L that was achieved under UV light of 18W intensity. Even at pH 3, the results of phenol degradation were more efficient using visible light in comparison to UV light due to fact of activation of $TiO_2$ under visible light after being sensitized by safranin dye.

Bukhari et al. (2019) studied the impacts of various parameters on the photocatalytic oxidation of slaughterhouse wastewater using $TiO_2$ and it was found that at acidic pH, removal rate was maximum due to fact that positive surface of $TiO_2$ efficiently adsorbs organic matter on its surface present in wastewater.

The presence of safranin played a significant role in the degradation of phenol because it was used in the process of sensitization which efficiently increased the photocatalytic activity of $TiO_2$. Safranin dye was used on the basis of the fact that it is a textile dye and could be extracted from textile wastewater to be used in wastewater treatment.

## 4.6 COD determination

### 4.6.1 COD determination under different light intensity

COD of the phenolic solution was measured in order to check the carbon content present in the wastewater which is considered to be the phenol solution of 50 mg/L. The rate of degradation is in inverse relation with the COD. As the rate of degradation increases, the value of COD decreases with the period of time. Determination of COD indirectly confirms the degradation rate of phenolic solution.

COD of the phenol solution was determined using both UV light (8W & 16W) and visible light (18W & 36W) to determine the carbon dioxide ($CO_2$) present in the solution, as the end product of the organic compound after photocatalytic degradation is $CO_2$ and water. Figure 4.30 shows the determined COD under UV light of intensities 8W and 16W.

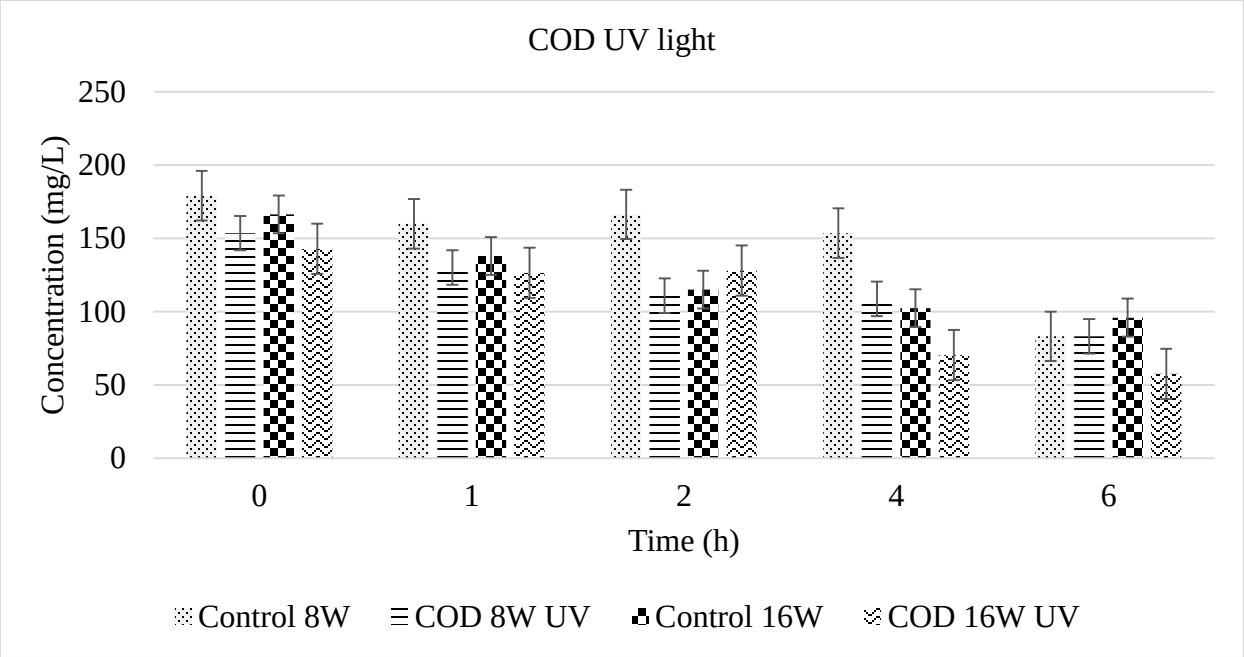


**Figure 4.30: COD determination of phenol solution under UV light of 8W and 16W**

As reported by Al-Hashemi et al. (2015), the range of COD in oil refineries is usually from 50-185 mg/L and for general wastewater the range of COD is usually from 10-100 mg/L. So, under UV light, the determined COD of control solution with no dye sensitized, the phenol solution exhibited the highest value of COD that indicated the low rate of degradation. Supporting the fact that with increase in degradation rate, COD rate decreases. COD value of the treatment (500 mg dye sensitized TNPs) under UV light of both intensities 8W and 16W was less than 200 mg/L. Figure 4.31 shows the determined COD of phenol solution under visible light of intensities 18W and 36W. Reason of phenolic solution COD not being decreased to levels below 20 mg/L or 10 mg/L might be due to the fact that after a certain period of time the phenol compounds will transform into its intermediate products causing the COD levels to remain under 100 mg/L.

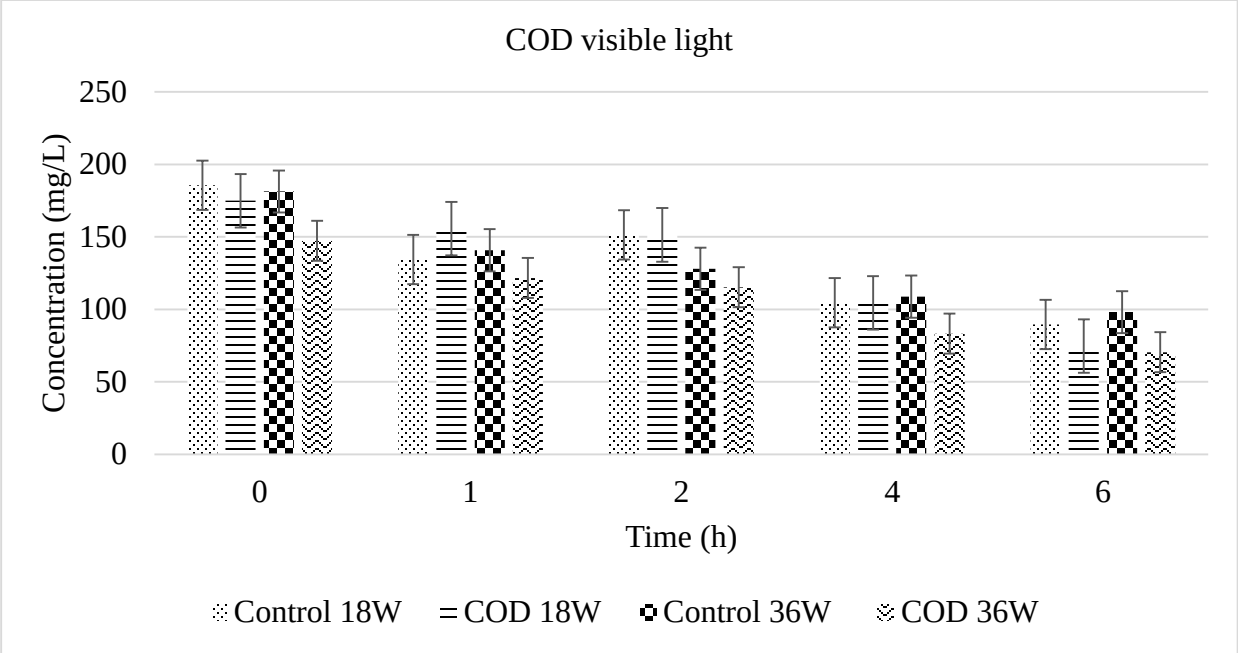


**Figure 4.31: COD determination of phenol solution under visible light of 18W and 36W**

### 4.6.2 COD determination under acidic pH

COD under acidic pH 3 was determined under the highest intensities of both UV and visible light which were 16W and 36W, respectively. Figure 4.32 shows the determination of COD under UV light of 16W at acidic pH 3.

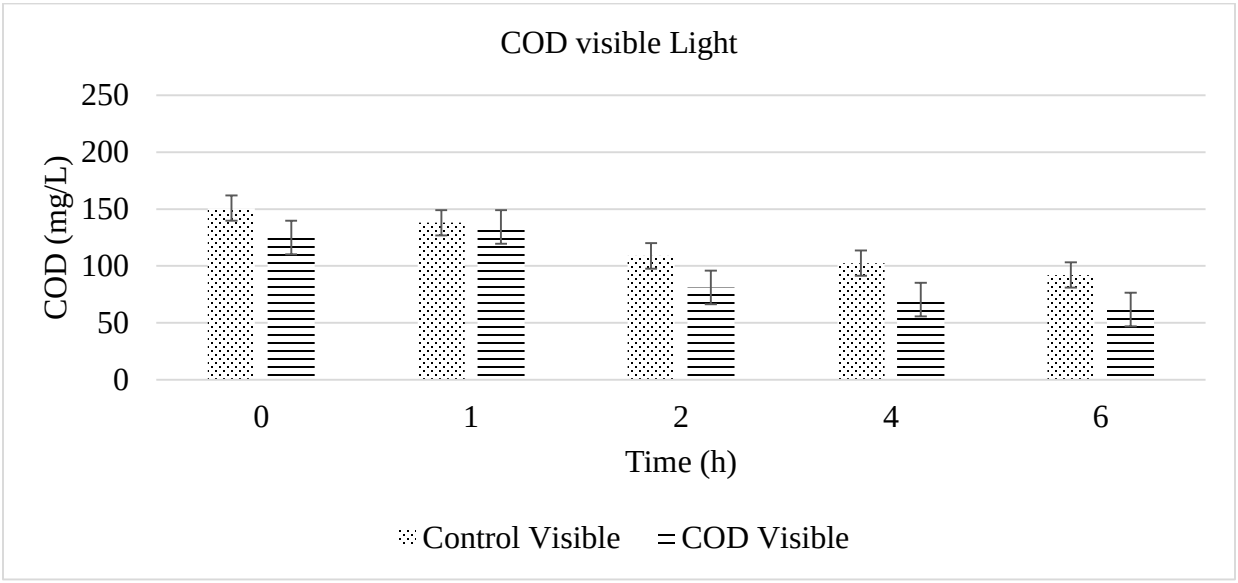


**Figure 4.32: COD determination of phenol solution at pH 3 under 16W UV light**

With the increasing period of time up to 6 h, the value of COD was decreased supporting the fact that rate of degradation was increased. In all of the study cases of COD, COD (mg/L) was plotted against the time starting from 0 min to 6 h at the x-axis. At pH 3, using UV light and visible light of both intensities level of COD was decreased to be under 100 mg/L, respectively.

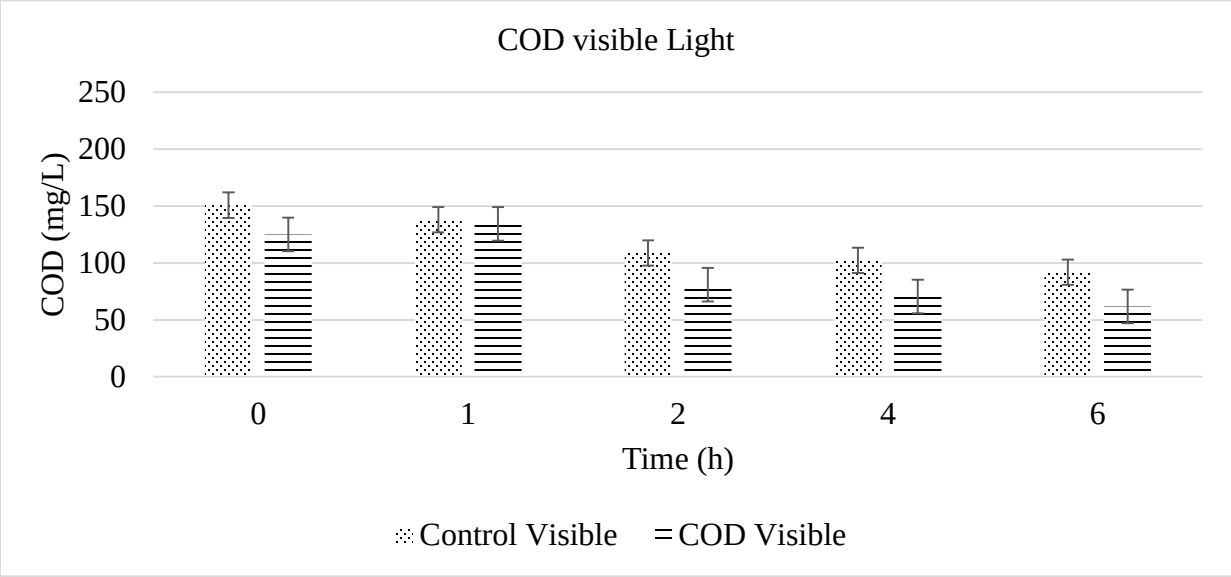


**Figure 4.33: COD determination of phenol solution at pH 3 under 36W visible light**

# 5 CONCLUSIONS AND RECOMMENDATIONS

## 5.1 Conclusions

Followings are conclusions drawn from the research done:

- Dye sensitization of $TiO_2$ nanoparticles has increased the degradation rate of phenol under visible light and such dye sensitized nanoparticles are likely to degrade under sunlight at a good rate.
- The optimum dosage of 500mg/500mL dye sensitized $TiO_2$ nanoparticles were able to degrade 50 mg/L concentration of phenol to 50%-60% under 36W intensity of visible light.
- It was found that at pH 3, 50 mg/L of phenol was degraded to 30%-40% under 36W intensity of visible light.
- The efficiency of dye sensitized $TiO_2$ nanoparticles was enhanced under visible light due to narrowing of the band gap energy.

## 5.2 Recommendations for Future work

Keeping in view of the results reported in this study, some suggestions are given below for future experimentations:

- Effect of other parameters such as alkaline pH and temperature can be studied on the degradation of phenol in future.
- Combination of biodegradation with photocatalytic degradation may be the most promising technology for the remediation of environmental pollutants in future.

## REFERENCES


Abd El-Gawad, H. S. (2014). Oil and Grease Removal from Industrial Wastewater Using New Utility Approach. *Advances in Environmental Chemistry*. *Article ID*, *916878*.

Abd Gami, A., Shukor, M. Y., Khalil, K. A., Dahalan, F. A., Khalid, A., & Ahmad, S. A. (2014). Phenol and its toxicity. *Journal of Environmental Microbiology and Toxicology*, *2*(1), 11-24.

Adeola, A. O. (2018). Fate and toxicity of chlorinated phenols of environmental implications: a review. *Medicinal and Analytical Chemistry International Journal*, *2*(4), 000126.

Ahmed, S., Rasul, M. G., Martens, W. N., Brown, R., & Hashib, M. A. (2010). Heterogeneous photocatalytic degradation of phenols in wastewater: a review on current status and developments. *Desalination*, *261*(1-2), 3-18.

Akpor, O. B., Otohinoyi, D. A., Olaolu, D. T., & Aderiye, B. I. (2014). Pollutants in wastewater effluents: impacts and remediation processes. *International Journal of Environmental Research and Earth Science*, *3*(3), 050-059.

Al Hashemi, W., Maraqa, M. A., Rao, M. V., & Hossain, M. M. (2015). Characterization and removal of phenolic compounds from condensate-oil refinery wastewater. *Desalination and Water Treatment*, *54*(3), 660-671.

Ali, S. S., Qazi, I. A., Arshad, M., Khan, Z., Voice, T. C., & Mehmood, C. T. (2016). Photocatalytic degradation of low density polyethylene (LDPE) films using titania nanotubes. *Environmental Nanotechnology, Monitoring & Management*, *5*, 44-53.

Al-Khalid, T., & El-Naas, M. H. (2017). Organic Contaminants in Refinery Wastewater: Characterization and Novel Approaches for Biotreatment. In *Recent Insights in Petroleum Science and Engineering*. IntechOpen.

Anku, W. W., Mamo, M. A., & Govender, P. P. (2017). Phenolic compounds in water: sources, reactivity, toxicity and treatment methods. *Phenolic compounds-natural sources, importance and applications*, 420-443.

Azizah, A. N., & Widiasa, I. N. (2018). Advanced oxidation processes (AOPs) for refinery wastewater treatment contains high phenol concentration. In *MATEC Web of Conferences* (Vol. 156, p. 03012). EDP Sciences.

Babich, H., & Davis, D. L. (1981). Phenol: A review of environmental and health risks. *Regulatory Toxicology and Pharmacology*, *1*(1), 90-109.

Balaji, G., Rekha, R. K., & Ramalingam, A. (2011). Nonlinear characterization of safranin O dye for application in optical limiting. *Acta Physica Polonica A*, *119*, 359-363.

Barakat, M. A., Al-Hutailah, R. I., Qayyum, E., Rashid, J., & Kuhn, J. N. (2014). Pt nanoparticles/TiO2 for photocatalytic degradation of phenols in wastewater. *Environmental Technology*, *35*(2), 137-144.

Behnajady, M. A., Modirshahla, N., Shokri, M., & Rad, B. (2008). Enhancement of photocatalytic activity of TiO2 nanoparticles by silver doping: photodeposition versus liquid impregnation methods. *Global NEST Journal*, *10*(1), 1-7.

Braslavsky, S. E., Houk, K. N., & Verhoeven, J. W. (1988). Glossary of terms used in photochemistry. *Pure Appl. Chem*, *60*, 1055-1106.

Brandão, Y. B., de Oliveira, J. G. C., & Benachour, M. (2017). Phenolic Wastewaters: Definition, Sources and Treatment Processes. *Phenolic Compounds: Natural Sources, Importance and Applications*, 323.

Braslavsky, S. E. (2007). Glossary of terms used in photochemistry, (IUPAC Recommendations 2006). *Pure and Applied Chemistry*, *79*(3), 293-465.

Bukhari, K., Ahmad, N., Sheikh, I. A., & Akram, T. M. (2019). Effects of different parameters on photocatalytic oxidation of slaughterhouse wastewater using TiO. *Polish Journal of Environmental Studies*, *28*(3), 1-10.

Bunaciu, A. A., UdriŞTioiu, E. G., & Aboul-Enein, H. Y. (2015). X-ray diffraction: instrumentation and applications. *Critical Reviews in Analytical Chemistry*, *45*(4), 289-299.

Chen, L., Wu, P., Chen, M., Lai, X., Ahmed, Z., Zhu, N., Dang, Z., Bi, Y., & Liu, T. (2018). Preparation and characterization of the eco-friendly chitosan/vermiculite biocomposite with excellent removal capacity for cadmium and lead. *Applied Clay Science*, *159*, 74-82.

Chen, M., Wu, P., Yu, L., Liu, S., Ruan, B., Hu, H., Zhu, N., & Lin, Z. (2017). FeOOH-loaded $MnO_2$ nano-composite: An efficient emergency material for thallium pollution incident. *Journal of Environmental Management*, *192*, 31-38.

Chiu, Y. H., Chang, T. F. M., Chen, C. Y., Sone, M., & Hsu, Y. J. (2019). Mechanistic insights into photodegradation of organic dyes using heterostructure photocatalysts. *Catalysts*, *9*(5), 430.

Chopra, R. (2016). Environmental degradation in India: causes and consequences. *International Journal of Applied Environmental Sciences*, *11*(6), 1593-1601.

Choquette-Labbé, M., Shewa, W. A., Lalman, J. A., & Shanmugam, S. R. (2014). Photocatalytic degradation of phenol and phenol derivatives using a nano-$TiO_2$ catalyst: Integrating quantitative and qualitative factors using response surface methodology. *Water*, *6*(6), 1785-1806.

Chowdhury, P., Moreira, J., Gomaa, H., & Ray, A. K. (2012). Visible-solar-light-driven photocatalytic degradation of phenol with dye-sensitized $TiO_2$: parametric and kinetic study. *Industrial & Engineering Chemistry Research*, *51*(12), 4523-4532.

Chowdhury, P., Nag, S., & Ray, A. K. (2017). Degradation of phenolic compounds through UV and visible-light-driven photocatalysis: technical and economic aspects. *Phenolic Compounds: Natural Sources, Importance and Applications*, *395*.

Dai, G., Chao, L. M., & Iwasa, T. (2014). Photocatalytic degradation of phenol with bacteriorhodopsin sensitized TiO2 nanoparticles. In *Advanced Materials Research* (Vol. 955, pp. 415-418). Trans Tech Publications Ltd.

Dang, T. T. T., Le, S. T. T., Channei, D., Khanitchaidecha, W., & Nakaruk, A. (2016). Photodegradation mechanisms of phenol in the photocatalytic process. *Research on Chemical Intermediates*, *42*(6), 5961-5974.

Diantoro, M., Kusumaatmaja, A., & Triyana, K. (2018, April). Study on Photocatalytic Properties of TiO2 Nanoparticle in various pH condition. In *Journal of Physics: Conference Series* (Vol. 1011, No. 1, p. 012069). IOP Publishing.

De Caro, C., & Haller, C. (2015). UV/VIS spectrophotometry-fundamentals and applications. *Mettler-Toledo International*, 4-14.

Dil, M. A., Haghighatzadeh, A., & Mazinani, B. (2019). Photosensitization effect on visible-light-induced photocatalytic performance of $TiO_2$/chlorophyll and flavonoid nanostructures: kinetic and isotherm studies. *Bulletin of Materials Science*, *42*(5), 248.

El-Kemary, M., & El-Shamy, H. (2009). Fluorescence modulation and photodegradation characteristics of safranin O dye in the presence of ZnS nanoparticles. *Journal of Photochemistry and Photobiology A: Chemistry*, *205*(2-3), 151-155.

Eskandarloo, H., & Badiei, A. (2014). Photocatalytic application of titania nanoparticles for degradation of organic pollutants. *Nanotechnology for Optics and Sensors*, 108-132.

Geissen, V., Mol, H., Klumpp, E., Umlauf, G., Nadal, M., van der Ploeg, M., ... & Ritsema, C. J. (2015). Emerging pollutants in the environment: a challenge for water resource management. *International Soil and Water Conservation Research*, *3*(1), 57-65.

Granados, G., Martínez, F., & Páez-Mozo, E. A. (2005). Photocatalytic degradation of phenol on $TiO_2$ and TiO2/Pt sensitized with metallophthalocyanines. *Catalysis today*, *107*, 589-594.

Griffiths, P. R., & De Haseth, J. A. (2007). *Fourier transform infrared spectrometry* (Vol. 171). John Wiley & Sons.

Gupta, S. M., & Tripathi, M. (2011). A review of $TiO_2$ nanoparticles. *Chinese Science Bulletin*, *56*(16), 1639.

Ghosh, M., Chowdhury, P., & Ray, A. K. (2020). Photocatalytic activity of aeroxide $TiO_2$ sensitized by natural dye extracted from mangosteen peel. *Catalysts*, *10*(8), 917.

Hanaor, D. A., & Sorrell, C. C. (2011). Review of the anatase to rutile phase transformation. *Journal of Materials Science*, *46*(4), 855-874.

Haghighatzadeh, A. (2020). Comparative analysis on optical and photocatalytic properties of chlorophyll/curcumin-sensitized $TiO_2$ nanoparticles for phenol degradation. *Bulletin of Materials Science*, *43*(1), 1-15.

Husnain, A., Qazi, I. A., Khaliq, W., & Arshad, M. (2016). Immobilization in cement mortar of chromium removed from water using titania nanoparticles. *Journal of Environmental Management*, *172*, 10-17.

Inkson, B. J. (2016). Scanning electron microscopy (SEM) and transmission electron microscopy (TEM) for materials characterization. In *Materials characterization using nondestructive evaluation (NDE) methods* (pp. 17-43). Woodhead Publishing.

Janitabar Darzi, S., & Movahedi, M. (2014). Visible light photodegradation of phenol using nanoscale $TiO_2$ and ZnO impregnated with merbromin dye: a mechanistic investigation. *Iranian Journal of Chemistry and Chemical Engineering (IJCCE)*, *33*(2), 55-64.

Kanan, S., Moyet, M. A., Arthur, R. B., & Patterson, H. H. (2020). Recent advances on $TiO_2$-based photocatalysts toward the degradation of pesticides and major organic pollutants from water bodies. *Catalysis Reviews*, *62*(1), 1-65.

Khan, S. A., Khan, S. B., Khan, L. U., Farooq, A., Akhtar, K., & Asiri, A. M. (2018). Fourier transform infrared spectroscopy: fundamentals and application in functional groups and nanomaterials characterization. In *Handbook of Materials Characterization* (pp. 317-344). Springer, Cham.

Khan, S., Qazi, I. A., Hashmi, I., Awan, M. A., & Zaidi, N. U. S. S. (2013). Synthesis of silver-doped titanium TiO2 powder-coated surfaces and its ability to inactivate pseudomonas aeruginosa and bacillus subtilis. *Journal of Nanomaterials*, *2013*.

Kumar, D. A., Shyla, J. M. and Xavier, F. P. (2018). Synthesis and Optical, Photoconductivity Study of Safranin O Dye Sensitized Titania/ Silica oxide system Prepared by Modified Sol-gel Method. *International Journal of Recent Technology and Engineering.* (7), 2277-3878.

Levchuk, I., & Sillanpää, M. (2020). Titanium dioxide–based nanomaterials for photocatalytic water treatment. In *Advanced Water Treatment* (pp. 1-56). Elsevier.

Levén, L., & Schnürer, A. (2010). Molecular characterisation of two anaerobic phenol-degrading enrichment cultures. *International Biodeterioration & Biodegradation*, *64*(6), 427-433.

Li Puma, G., & Yue, P. L. (2002). Effect of the radiation wavelength on the rate of photocatalytic oxidation of organic pollutants. *Industrial & Engineering Chemistry Research*, *41*(23), 5594-5600.

Liu, J., Wu, P., Li, S., Chen, M., Cai, W., Zou, D.,Zhu, N., & Dang, Z. (2019). Synergistic deep removal of As (III) and Cd (II) by a calcined multifunctional MgZnFe-$CO_3$ layered double hydroxide: photooxidation, precipitation and adsorption. *Chemosphere*, *225*, 115-125.

Mahlambi, M. M., Ngila, C. J., & Mamba, B. B. (2015). Recent developments in environmental photocatalytic degradation of organic pollutants: the case of titanium dioxide nanoparticles—a review. *Journal of Nanomaterials*, *2015*.

Mangrola, M. H., Parmar, B. H., Pillai, A. S., & Joshi, V. S. (2012). Structural, optical and electrical properties of titanium dioxide nanoparticle. *Multi-Disciplinary Edu Global Quest*, *1*, 138-145.

Mele, G., Ciccarella, G., Vasapollo, G., García-López, E., Palmisano, L., & Schiavello, M. (2002). Photocatalytic degradation of 4-nitrophenol in aqueous suspension by using polycrystalline

TiO2 samples impregnated with Cu (II)-phthalocyanine. *Applied Catalysis B: Environmental*, *38*(4), 309-319.

Mohammed, A., & Abdullah, A. (2018, November). Scanning electron microscopy (SEM): A review. In *Proceedings of the 2018 International Conference on Hydraulics and Pneumatics—HERVEX, Băile Govora, Romania* (pp. 7-9).

Murcia Mesa, J. J., García Arias, J. A., Rojas, H. A., & Cárdenas Espinosa, O. E. (2020). Photocatalytic degradation of Phenol, Catechol and Hydroquinone over Au-ZnO nanomaterials. *Revista Facultad de Ingeniería Universidad de Antioquia*, (94), 24-32.

Patel, N. H. (2015). Basic Principle, Working and Instrumentation of Experimental Techniques.57-101.

Pirbazari, A. E. (2017). Photocatalytical Treatment of Synthetic Wastewater Containing Chlorophenols by TiO2 Nanoparticles Sensitized with Cobalt Phthalocyanine Under Visible Light. *J Chem Eng Process Technol*, *8*(333), 26-30.

Rafiee, E., Noori, E., Zinatizadeh, A. A., & Zanganeh, H. (2016). Photocatalytic degradation of phenol using a new developed TiO 2/Graphene/Heteropoly acid nanocomposite: Synthesis, characterization and process optimization. *RSC advances*, *6*(99), 96554-96562.

Rashid, J., Barakat, M. A., Pettit, S. L., & Kuhn, J. N. (2014). InVO 4/$TiO_2$ composite for visible-light photocatalytic degradation of 2-chlorophenol in wastewater. *Environmental Technology*, *35*(17), 2153-2159.

Rezaei, B., & Mosaddeghi, H. (2006, February). Applications of titanium dioxide nanocoating. In *Nano-technology in Environments Conference* (p. 6).

Riaz, S., & Naseem, S. (2015). Controlled nanostructuring of $TiO_2$ nanoparticles: a sol–gel approach. *Journal of Sol-Gel Science and Technology*, *74*(2), 299-309.

Safaralizadeh, E., Darzi, S. J., Mahjoub, A. R., & Abazari, R. (2017). Visible light-induced degradation of phenolic compounds by Sudan black dye sensitized $TiO_2$ nanoparticles as an advanced photocatalytic material. *Research on Chemical Intermediates*, *43*(2), 1197-1209.

Sarathi, P., & Thilagavathi, G. (2009). Synthesis and characterization of titanium dioxide nano-particles and their applications to textiles for microbe resistance. *Journal of Textile and Apparel, Technology and Management*, *6*(2).

Setiawati E, Kawano K. Stabilization of anatase phase in the rare earth; Eu and Sm ion doped

Shahrezaei, F., Akhbari, A., & Rostami, A. (2012). Photodegradation and removal of phenol and phenolic derivatives from petroleum refinery wastewater using nanoparticles of TiO2. *International Journal of Energy and Environment*, *3*(2), 267-274.

Shahrezaei, F., Akhbari, A., & Rostami, A. (2012). Photodegradation and removal of phenol and phenolic derivatives from petroleum refinery wastewater using nanoparticles of TiO2. *International Journal of Energy and Environment*, *3*(2), 267-274.

Singh, T., Bhatiya, A. K., Mishra, P. K., & Srivastava, N. (2020). An effective approach for the degradation of phenolic waste: phenols and cresols. In *Abatement of Environmental Pollutants* (pp. 203-243). Elsevier.

Sulaiman, F., Sari, D. K., & Kustiningsih, I. (2017, May). The influence of ozone on the photocatalytic degradation of phenol using TiO2 photocatalyst supported by Bayah natural zeolite. In *AIP Conference Proceedings* (Vol. 1840, No. 1, p. 110014). AIP Publishing LLC.

Suzuki, H., Araki, S., & Yamamoto, H. (2015). Evaluation of advanced oxidation processes (AOP) using O3, UV, and $TiO_2$ for the degradation of phenol in water. *Journal of Water Process Engineering*, *7*, 54-60.

Theivasanthi, T., & Alagar, M. (2013). Titanium dioxide ($TiO_2$) nanoparticles XRD analyses: an insight. *arXiv preprint arXiv:1307.1091*.

Vaiano, V., Sacco, O., Sannino, D., Stoller, M., Ciambelli, P., & Chianese, A. (2016). Photocatalytic removal of phenol by ferromagnetic N-$TiO_2$/$SiO_2$/$Fe_3O_4$ nanoparticles in presence of visible light irradiation. *Chemical Engineering Transactions*, *47*, 235-240.

Varadaraju, C., Tamilselvan, G., Enoch, I. M. V. M., & Selvakumar, M. (2018). Phenol sensing studies by 4-aminoantipyrine method—a review. *Organic and Medical Chemistry*, *5*(2), 1-7.

Wang, G., Xu, D., Guo, W., Wei, X., Sheng, Z., & Li, Z. (2017, March). Preparation of $TiO_2$ nanoparticle and photocatalytic properties on the degradation of phenol. In *IOP Conference Series: Earth and Environmental Science* (Vol. 59, No. 1, p. 012046). IOP Publishing.

Yunus, N. N., Hamzah, F., So'Aib, M. S., & Krishnan, J. (2017, June). Effect of catalyst loading on photocatalytic degradation of phenol by using N, S Co-doped $TiO_2$. In *IOP Conference Series: Materials Science and Engineering* (Vol. 206, No. 1, p. 012092). IOP Publishing.

Zhang, S., Li, L., & Kumar, A. (2008). *Materials characterization* techniques. CRC press.

Zyoud, A. H., Saleh, F., Helal, M. H., Shawahna, R., & Hilal, H. S. (2018). Anthocyanin-Sensitized $TiO_2$ Nanoparticles for Phenazopyridine Photodegradation under Solar Simulated Light. *Journal of Nanomaterials*, *2018*. http://dx.doi.org/10.1155/2014/968298

Zangeneh, H., Zinatizadeh, A. A. L., Habibi, M., Akia, M., & Isa, M. H. (2015). Photocatalytic oxidation of organic dyes and pollutants in wastewater using different modified titanium dioxides: A comparative review. *Journal of Industrial and Engineering Chemistry*, *26*, 1-36.